RSC Advances

PAPER

View Article Online
View Journal | View Issue

Check for updates

Cite this: *RSC Adv.*, 2025, **15**, 21962

Design, synthesis, *in silico* and *in vitro* evaluation of pyrrole–indole hybrids as dual tubulin and aromatase inhibitors with potent anticancer activities†

Rungroj Saruengkhanphasit, *[ab] Jaruwan Chatwichien, [ac] Lukana Ngiwsara, [d] Kriengsak Lirdprapamongkol, [bd] Worawat Niwetmarin, [a] Chatchakorn Eurtivong, *[e] Prasat Kittakoop, [abf] Jisnuson Svasti [d] and Somsak Ruchirawat [abg]

Twenty-four new pyrrolyl-3-phenyl-1*H*-indole-2-carbohydrazide derivatives were designed, synthesized and evaluated for their anticancer activities and dual inhibition properties against tubulin and aromatase. Their anticancer activities were highly potent against the NCI60 human cancer cell line panel. Amongst them, single chloro-substituted derivative **3h** was the strongest tubulin inhibitor, disrupting the microtubule structure by inhibiting the colchicine site, while potently inhibiting aromatase (IC_{50} = 1.8 μM) with strong activity against the estrogen receptor-positive T47D breast cancer cell line (IC_{50} = 2.4 μM). Ester derivative **3k** showed the best aromatase inhibitory activity (IC_{50} = 18 nM) with moderate anti-T47D activity (IC_{50} = 10.6 μM). Molecular docking predicted the derivatives inhibited the colchicine site of tubulin by forming mainly hydrophobic interactions with the surrounding amino acid residues. Moreover, heme chelation with the pyrrole ring was predicted as a key interaction, and the formation of intermolecular bonds with adjacent amino acid residues was predicted as important for inhibitory activity.

Received 25th December 2024
Accepted 23rd June 2025

DOI: 10.1039/d4ra09000d

rsc.li/rsc-advances

Open Access Article. Published on 27 June 2025. Downloaded on 12/13/2025 6:15:48 PM.
This article is licensed under a Creative Commons Attribution 3.0 Unported Licence.

1. Introduction

Cancer has been reported by the World Health Organization (WHO) as a leading cause of death, with almost 10 million deaths in 2020.[1] Furthermore, the WHO estimated that there would be around 20 million new cancer cases and 9.7 million deaths globally in 2022, and also projected that by 2050, there would be a 77% increase in new cases.[2] Statistics revealed that lung (12.6%), breast (11.6%), and colon (9.6%) cancers were the first, second and third most common types of new cases in 2022, respectively.[2] In the same report, lung cancer was the most common cause of deaths at 18.7% followed by colon cancer at 9.3%, and liver cancer and breast cancer at 7.8% and 6.9%, respectively. These statistics clearly indicate that cancer is a major global health burden.[2]

Estrogen receptor-positive (ER+) breast cancer is the most prevalent type of breast cancer, and is characterized by the predominant expression of estrogen and progesterone receptors, which drives cell proliferation in the breast.[3] The chemotherapeutic approach to treat ER+ breast cancer is mainly by administration of hormonal drugs, *i.e.*, selective estrogen receptor modulators (SERMs), selective estrogen receptor degrader (SERD) and aromatase inhibitors to suppress estrogenic signals.[4] Aromatase is a cytochrome P450 enzyme that contains a heme cofactor that is central to the catalytic conversion of androgens into estrogens.[3] Aromatase activity is often upregulated in ER+ breast cancer tissues and has been designated as a key drug target for many clinically approved aromatase inhibitors: exemestane, letrozole and anastrozole (Fig. 1).[3] Despite their clinical effectiveness, they are currently being challenged by drug resistance and undesirable side effects in patients, such as musculoskeletal pain, osteoporosis and cardiovascular problems.[5–8] Other anticancer agents used to treat breast cancers include drugs that modulate microtubule

[a]*Chulabhorn Graduate Institute, Program in Chemical Sciences, 54 Kamphaeng Phet 6, Talat Bang Khen, Lak Si, Bangkok 10210, Thailand. E-mail: rungrojs@cgi.ac.th; Tel: +66 25541900 ext. 2629*

[b]*Center of Excellence on Environmental Health and Toxicology (EHT), OPS, Ministry of Higher Education, Science, Research and Innovation, Bangkok, Thailand*

[c]*Chulabhorn Royal Academy, Bangkok 10210, Thailand*

[d]*Laboratory of Biochemistry, Chulabhorn Research Institute, Bangkok, 10210, Thailand*

[e]*Department of Pharmaceutical Chemistry, Faculty of Pharmacy, Mahidol University, 447 Si Ayutthaya Road, Ratchathewi, Bangkok 10400, Thailand. E-mail: chatchakorn.eur@mahidol.edu; Tel: +66 26448677-91 ext. 5402*

[f]*Laboratory of Natural Products, Chulabhorn Research Institute, Bangkok 10210, Thailand*

[g]*Laboratory of Medicinal Chemistry, Chulabhorn Research Institute, Bangkok 10210, Thailand*

† Electronic supplementary information (ESI) available. See DOI: https://doi.org/10.1039/d4ra09000d

© 2025 The Author(s). Published by the Royal Society of Chemistry

Open Access Article. Published on 27 June 2025. Downloaded on 12/13/2025 6:15:48 PM.
This article is licensed under a Creative Commons Attribution 3.0 Unported Licence.

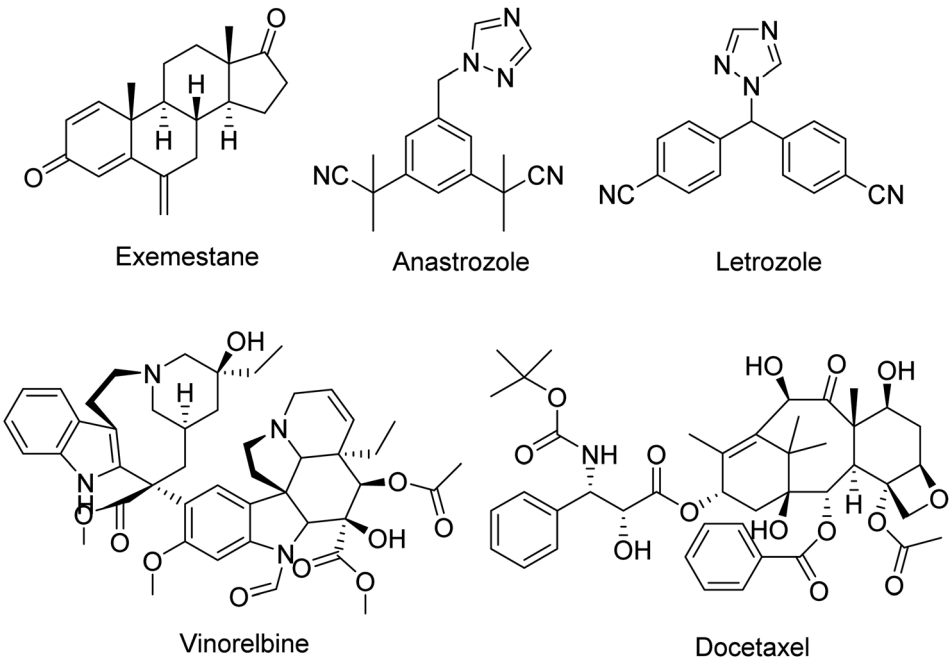

Fig. 1 The chemical structures of clinically approved aromatase inhibitors (exemestane, anastrozole and letrozole), and microtubule-modulating agents (vinorelbine and docetaxel) for breast cancer treatment.

activities such as vinorelbine and docetaxel (Fig. 1), which belong to the *Vinca* alkaloid and taxane classes of drugs, respectively.[9] Microtubule-modulating agents exert their mechanism of action by binding to tubulin monomers that interfere with microtubule dynamics during mitosis, subsequently leads to mitotic arrest.[9] Although clinically effective, they are limited by their large size, and are administered *via* injection and non-oral routes leading to inconvenience and compliancy issues for patients. Furthermore, cases of multidrug resistance were observed through various mechanisms, such as overexpression of drug efflux transporter MDR-1 (P-glycoprotein) resulting in reduced drug presence in cancer cells, and alteration of signal transduction pathways.[10] Given these drawbacks, there is a need for the discovery and development of new anti-breast cancer agents with orally acceptable pharmacokinetic profiles.

It has been observed that co-administration of aromatase inhibitor and microtubule-modulating drugs can improve clinical effectiveness in breast cancer patients.[11,12] Despite of these positive outcomes, such combinations can increase the risk of adverse effects, drug interactions, and detrimental physiological change. An alternative approach is to use dual-targeting strategies by employing dual-targeting agents, *i.e.*, agents that simultaneously interact with two different targets or pathways. This strategy has been applied broadly in medicinal chemistry with proven enhanced pharmacological potencies, clinical effectiveness and to overcome multidrug resistance mechanisms, *e.g.* antitubercular agents,[13,14] anti-Alzheimer's agents,[15,16] antimalarials,[17] anti-rheumatics[18] and anticancer agents.[19–23] Regardless of the potential benefits, marginal development of agents that modulate aromatase and tubulin activities were reported such as the 1-(diarylmethyl)-1*H*-azoles series,[24] whereas, dual modulators of tubulin and estrogen receptor activities have shown slightly more traction, *e.g.*, modulation of tubulin and antagonism of estrogen receptors.[25,26]

In our previous work, we have identified furanyl derivatives **1a**, and thiophenyl derivatives **2a** as promising anticancer agents, which subsequently led to the synthesis of **1b** and **2b** (Fig. 2) that exhibited potent anti-tubulin and anticancer activities.[27,28] Typically, it was revealed that several derivatives from the thiophenyl subseries, including **2b**, displayed potent antiproliferative activities and selectivity for certain cancer cell lines.[28] The series is based on the 3-phenyl-1*H*-indole-2-carbohydrazide as the core scaffold. Consequently, this scaffold was used in this work as a platform for the design of new anticancer agents. Prior to this work, we were interested in attaching a pyrrole ring to our core scaffold, since pyrrole is a natural chelator of metals in many biological structures such as magnesium in chlorophyll, heme iron in hemoglobin and cytochrome P450 enzymes, including aromatase. Given this rationale, the pyrrole ring was attached to the side chain of the 3-phenyl-1*H*-indole-2-carbohydrazide core scaffold affording **3a** (Fig. 2) with the expectation of a dual-targeting mechanism, *i.e.*, tubulin and aromatase inhibition. This was followed by establishing a preliminary structure–activity relationship (SAR) by the synthesis of twenty-four new derivatives with various substituents installed at the pyrrole ring followed by experimental validation of their anticancer, anti-tubulin, and anti-aromatase activities. Furthermore, molecular modeling was employed to gain an understanding of the interactions between the compounds and the protein targets, and their

Open Access Article. Published on 27 June 2025. Downloaded on 12/13/2025 6:15:48 PM. This article is licensed under a Creative Commons Attribution 3.0 Unported Licence.

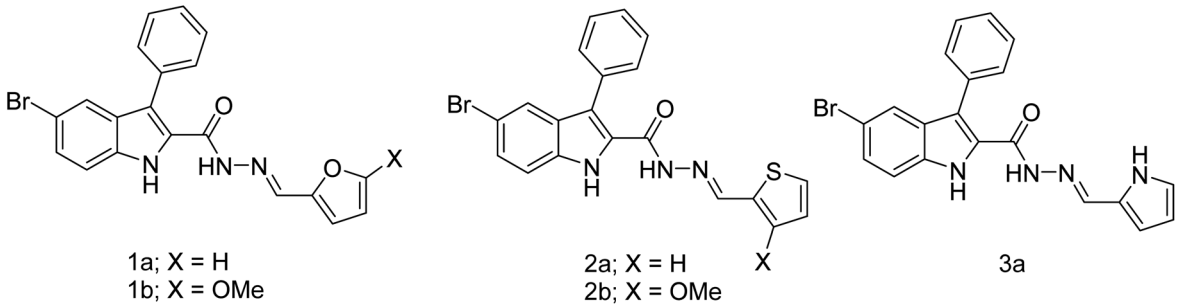

Fig. 2 The chemical structures of compounds **1a–b**, **2a–b**, and **3a**.

physicochemical properties were evaluated. It should be noted that previously, aryl-substituted derivatives were synthesised by Cai and co-workers,[29] however these derivatives displayed only weak anticancer effects, Moreover, cycloalkyl derivatives were previously prepared by our groups, but they exhibited poor anticancer activities.[27] The present work focuses on anticancer pyrrole–indole hybrids with dual tubulin and aromatase inhibitory activities.

2. Results and discussion

2.1. Chemistry

The synthesis of pyrrolyl-3-phenyl-1*H*-indole-2-carbohydrazide **3a–x** was achieved by the condensation of hydrazide **5** (ref. 28) with various pyrrole aldehyde (Scheme 1). The synthesis was initiated by replacing the ethoxy group of indole **4** (ref. 27) with hydrazine. Condensation of hydrazide **5** under acid condition with various substituted aldehydes afforded indole hydrazides. The indole hydrazide products from the condensation reaction could generate mixtures of *E*- and *Z*-isomers, but the *E*-isomer was isolated due to its high stability.[27,28]

The dimethyl substitutions at positions X_2 and X_4 on the pyrrole ring gave **3c**, whereas *N*-methyl afforded **3d**. The halogen-containing derivatives include bromo at X_3 (**3e**), dibromo (**3f**) at X_2 and X_3, single chloro substitution at X_4 (**3g**) and X_3 (**3h**). The electron-withdrawing groups were introduced for ester substitution at X_2 (**3i**), X_3 (**3j**), and X_4 (**3k**), carboxylic acid at X_2 (**3l**) and X_3 (**3m**), morpholine-4-carbonyl at positions X_2 (**3n**), and X_3 (**3o**), and nitro at positions X_2 (**3p**) and position X_3 (**3q**). Nitro substitution at X_3 and dimethyl at X_2 and X_4 positions generated **3r**. Weak electron-donating ethyl group was introduced at positions X_2 (**3s**), X_3 (**3t**), and X_4 (**3u**). Altering the connectivity from 2-pyrrolyl to 3-pyrrolyl afforded **3b**, and varying the functionality at position X produced ester (**3v**), carboxylic acid (**3w**), and amide (**3x**) derivatives. The purity of the compounds was assessed by ^{1}H NMR spectroscopy, which showed the purity of *ca.* 93–97% of the final products. The ^{1}H NMR spectra of some compounds have additional peaks due to the existence of rotamers arising from the amide bond rotation. To prove the existence of rotamers of these compounds, compounds **3d**, **3i**, and **3p** were selected for the ^{1}H NMR experiment at 90 °C (see ^{1}H and ^{13}C spectra in ESI†). Indeed, ^{1}H NMR spectra of compounds **3d**, **3i**, and **3p** at 90 °C showed only one set of a single isomer, confirming the presence of rotamers.

2.2. Biological evaluation

2.2.1. Anticancer activities. In order to evaluate the anticancer effects of derivatives **3a–x**, the derivatives were submitted to the NCI60 screening program.[30] Firstly, the derivatives were screened at the 10 μM single dose against the NCI60 human cell line panel. The results of the single dose experiment are reported as the growth percentage against each cell line together with mean growth inhibition (NCI mean) are reported (Fig. S1†). Most of the derivatives displayed strong antiproliferative effects in the single dose experiment with NCI mean values ranging from −10.66 to 29.76. Candidates that displayed potent anticancer activities were selected for the five-dose experiment to derive the concentrations that inhibit cell growth by 50% (GI_{50}) and kill cells by 50% (LC_{50}) values; the complete data are shown in Table S2 and Fig. S3.†

The pyrrole derivatives are mostly strong anticancer agents (GI_{50} < 1 μM), with some exhibiting strong lethal effects (LC_{50} < 10 μM). The parent compound **3a** displayed strong growth inhibition, and was most lethal against five cancer cell lines: HT29 colon adenocarcinoma (LC_{50} = 9.31 μM), UAAC-62 melanoma (LC_{50} = 8.03 μM), OVCAR-8 ovarian carcinoma (LC_{50} = 6.55 μM), SN12C renal cell carcinoma (LC_{50} = 3.97 μM), and BT-549 breast carcinoma (LC_{50} = 6.39). Derivative **3c** exhibited moderate growth inhibition activities with GI_{50} values between 1.77 and 8.25 μM, and was most lethal against SK-MEL-5 melanoma cell line (LC_{50} = 19.3 μM). Derivative **3d** displayed potent growth inhibition activities and was best at suppressing growth of MCF-7 breast cancer cells at double-digit nanomolar potency (GI_{50} = 72 nM), whilst exhibited selectivity for NCI/ADR-RES doxorubicin-resistant ovarian cancer cell line (LC_{50} = 40.9 μM) that overexpresses MDR1 drug efflux transporter.[31] Single bromo-substituted derivative **3e** displayed potent growth inhibition and exhibited most potent lethal effects against COLO 205 (LC_{50} = 0.89 μM), HT29 (LC_{50} = 8.24 μM), LOX IMVI (LC_{50} = 6.98 μM), SK-MEL-5 (LC_{50} = 1.22 μM), NCI/ADR-RES (LC_{50} = 0.97 μM), and SN12C (LC_{50} = 5.49 μM) cancer cell lines, whereas dibromo-substituted derivative **3f** displayed moderate growth inhibition effects with GI_{50} values ranging between 0.53 to 6.8 μM, and was potent at killing SK-MEL-5 (LC_{50} = 8.65 μM) and NCI/ADR-RES (LC_{50} = 9.73 μM). Single chloro-substituted derivatives **3g** and **3h** were effective at suppressing growth inhibition, albeit **3g** was less lethal. Derivative **3h** displayed potent lethal effects against HL-60 (TB), K-562 and SR leukemia, NCI-H460 non-small cell lung carcinoma, COLO

© 2025 The Author(s). Published by the Royal Society of Chemistry

Open Access Article. Published on 27 June 2025. Downloaded on 12/13/2025 6:15:48 PM.
This article is licensed under a Creative Commons Attribution 3.0 Unported Licence.

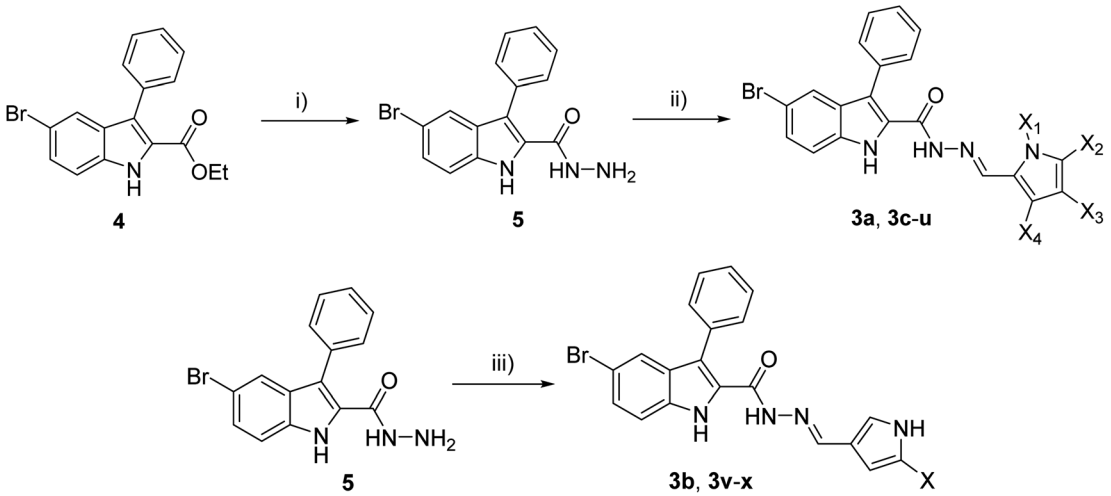

Derivative	X_1	X_2	X_3	X_4	% Yield
3a	H	H	H	H	95
3c	H	Me	H	Me	68
3d	Me	H	H	H	57
3e	H	H	Br	H	95
3f	H	Br	Br	H	96
3g	H	H	H	Cl	quantitative
3h	H	H	Cl	H	38
3i	H	CO_2Et	H	H	96
3j	H	H	CO_2Et	H	69
3k	H	H	H	CO_2Et	83
3l	H	CO_2H	H	H	60
3m	H	H	CO_2H	H	58
3n	H	$CON(C_2H_4)_2O$	H	H	81
3o	H	H	$CON(C_2H_4)_2O$	H	94
3p	H	NO_2	H	H	74
3q	H	H	NO_2	H	46
3r	H	Me	NO_2	Me	77
3s	H	Et	H	H	96
3t	H	H	Et	H	88
3u	H	H	H	Et	92

Derivative	X	% Yield
3b	H	86
3v	CO_2Et	60
3w	CO_2H	69
3x	$CON(C_2H_4)_2O$	83

Scheme 1 Synthesis of indole hydrazide derivatives; reagent and conditions: (i) N_2H_4, EtOH, 80 °C, 17 h, 70%; (ii) ArCHO, few drops AcOH, EtOH, 80 °C, 17 h, 46–100%; (iii) ArCHO, few drops AcOH, EtOH, 80 °C, 17 h, 67%.

205, HCC-2998 and HT29 colon carcinoma cell lines, SK-MEL-5 melanoma, and OVCAR-8 ovarian carcinoma with LC_{50} values in the range of 0.80 to 7.20 μM. Introduction of electron-withdrawing ester groups to derivatives **3i** and **3j** resulted in moderate growth inhibition activities. Nevertheless, **3i** showed strong lethal effects against SK-MEL-5 (LC_{50} = 7.68 μM) and NCI/ADR-RES cell lines (LC_{50} = 9.2 μM), and **3j** was potent against HL-60 (TB) (LC_{50} = 9.88 μM). Ester derivative **3k**, and the carboxylic acid derivatives **3l** and **3m** were opted out from the five-dose experiment, *i.e.*, **3k** displayed moderate growth inhibition (NCI mean = 49%), whereas **3l** and **3m** exhibited mild effects. Morpholine-4-carbonyl derivative **3n** was potent at growth suppression and exhibited potent lethality against HL-60 (TB) with LC_{50} = 8.56 μM, whereas **3o** showed moderate growth inhibition (NCI mean = 45%), and was subsequently excluded from the five-dose experiment. Single electron-

Open Access Article. Published on 27 June 2025. Downloaded on 12/13/2025 6:15:48 PM. This article is licensed under a Creative Commons Attribution 3.0 Unported Licence.

withdrawing nitro-substituted derivatives **3p** and **3q** showed potent growth inhibition effects; **3p** was most lethal against COLO 205 (LC_{50} = 8.08 μM) and SK-MEL-5 (LC_{50} = 8.69 μM), and **3q** was most selective for U251 glioblastoma (LC_{50} = 66.8 μM), as well as MDA-MB-435 melanoma (LC_{50} = 8.78 μM) and SK-MEL-5 melanoma (LC_{50} = 69.9 μM). Derivative **3r** exhibited moderate growth inhibition activities, but displayed lethal effects against NCI-H460, COLO 205, HT29, LOX IMVI, SK-MEL-5, NCI/ADR-RES and SN12C cell lines. Ethyl-substituted derivatives **3s**, **3t** and **3u** exhibited strong growth inhibition activities with moderate lethal effects for **3s** and **3u**, whilst **3t** displayed potent lethal effects for LOX IMVI and SK-MEL-5 melanoma cell lines, and MDA-MB-468 breast carcinoma. Altering the connectivity of the pyrrole ring resulted in apparent reduction in growth inhibition activities (**3a** *vs.* **3b**) with moderate lethal activities for most cell lines. The ester derivative **3v** exhibited strong lethal effects for MDA-MB-435 melanoma with LC_{50} = 9.35 μM, and the substituted carboxylic acid (**3w**) and morpholine-4-carbonyl (**3x**) derivatives displayed moderate growth inhibition in the single dose experiment with NCI mean values ranging between 66–68%.

Six derivatives were the most potent: compound **3a**, single electron-donating chloro- (**3e**) and bromo- (**3h**) substituted derivatives at X_2 position, a single nitro-substituted derivative **3p** at X_1 position, and a dimethylated and nitro-substituted derivative **3r**, and an ethylated derivative **3t** at X_2 position (Table 1). Small electron-donating and withdrawing substituents are favored for the anticancer effects, whereas derivatives with larger electron-withdrawing groups such as carbonyl-substituted derivatives are unfavorable. This can be attributed to an increase in molecular size and change in molecular shape which affects target binding. Additionally, an increase in molecular size and polarity perturbs drug-like behavior, *e.g.*, decrease passive diffusion of drugs into cancer cells. Comparing the NCI60 screening results from this work with our previous studies on the furanyl and thiophenyl derivatives, all three subseries possess strong efficacies for COLO 205 colon carcinoma, SK-MEL-5 and MDA-MB-435 melanoma, and OVCAR-8 ovarian carcinoma suggesting part of the mechanism of action is influenced by the presence of the same core scaffold.[28] Interestingly, **3d** displayed selectivity for the NCI/ADR-RES cell line, suggesting it as a highly promising candidate to treat multidrug-resistant ovarian cancers. In addition, **3q** was revealed to be the most selective at killing MDA-MB-435 and SK-MEL-5 melanoma cell lines implying it as an appealing candidate for invasive forms of melanoma treatment. Moreover, **3q** was identified to be relatively potent against U251 glioblastoma, which is highly associated with acquired drug resistance CNS cancer.[32]

2.2.2. Tubulin polymerization inhibition. The 3-phenyl-1*H*-indole-2-carbohydrazide core scaffold has been previously identified to have tubulin inhibition properties.[27–29] To investigate the mechanism of action of the new derivatives, eleven derivatives were selected to be tested in a tubulin polymerization inhibition assay (**3a–b**, **3d–e**, **3g–h**, **3p–q**, and **3s–u**). Colchicine (10 μM) and paclitaxel (3 μM) was used as positive controls (Fig. 3). From the results, **3h** was the most potent tubulin inhibitor with RFU ∼ 40 arbitrary units. Derivatives **3e** and **3p** were equally the second most potent inhibitors exhibiting tubulin inhibition at RFU ∼ 50 arbitrary units. This is followed by **3a**, **3s** and **3t** with moderate inhibition activities at RFU ∼ 55 arbitrary units. Derivatives **3b**, **3d**, **3g** and **3u** were weak tubulin inhibitors, and **3q** had no tubulin inhibition properties. The results showed poor correlations with the NCI60 data, suggesting that tubulin inhibition is not the primary mechanism of action.

2.2.3. Cell cycle analysis. Disruption of tubulin polymerization has been shown to cause the arrest of cell division at the G2/M phase of the cell cycle.[27] This drew our curiosity to study the effects of the series on cell cycle progression, so we used the strongest tubulin inhibitor, **3h**, to study the effects of cell cycle progression against the A549 non-small cell lung cancer cell line as a model. By treating with varying concentrations of **3h** (0.5–10.0 μM) for 24 h, morphological changes were observed. There was a decrease in cell density, while the number of spherical cells increased in a dose-dependent fashion (Fig. 4A) indicating an increase of cell population in the mitotic phase. This suggested that **3h** was able to induce cell cycle arrest.[33] Results showed that **3h** dose-dependently increased G2/M cell population to 42.4–77.1% of total cells, compared to 29.3% in the control group (Fig. 4B and C) indicating arrest at G2/M phase.

2.2.4. Aromatase inhibitory activity. All derivatives were tested for aromatase inhibition (Table 2); active derivatives are defined as derivatives with IC_{50} < 12.5 μM. In Table 2, the pyrrolyl derivatives displayed potent aromatase inhibitory activities with IC_{50} values ranging between 18 nM to double digit

Table 1 Dose–response for the most active derivatives shown for eight sensitive cancer cell lines in micro-molar (μM) concentrations

	3a		**3e**		**3h**		**3p**		**3r**		**3t**	
	GI_{50}	LC_{50}	GI_{50}	LC_{50}	GI_{50}	LC_{50}	GI_{50}	LC_{50}	GI_{50}	LC_{50}	GI_{50}	LC_{50}
HL-60 (TB)	0.242	>100	0.327	>100	0.185	0.886	0.374	>100	2.31	>100	0.237	91.9
COLO 205	0.261	35.1	0.192	0.884	0.251	1.88	1.52	8.08	1.9	7.51	0.207	—
LOX IMVI	0.244	19	0.36	6.98	0.37	16.7	0.519	35.8	1.63	5.73	0.427	8.27
MDA-MB-435	0.105	—	0.207	24.3	0.185	—	0.253	29.8	1.77	17.9	0.23	38.7
SK-MEL-5	0.302	15.7	0.195	1.22	0.228	3.08	1.02	8.69	1.5	5.87	0.279	6.96
OVCAR-8	0.323	6.55	0.304	18.2	0.214	0.988	1.02	39	3.08	36.5	0.316	26
NCI/(ADR-RES)	0.44	59.2	0.197	0.971	0.2	—	0.285	16.2	1.89	9.15	0.247	22
SN12C	0.371	3.97	0.310	5.49	0.391	15.3	1.24	36.7	1.74	6.73	0.372	30

© 2025 The Author(s). Published by the Royal Society of Chemistry

Open Access Article. Published on 27 June 2025. Downloaded on 12/13/2025 6:15:48 PM.
This article is licensed under a Creative Commons Attribution 3.0 Unported Licence.

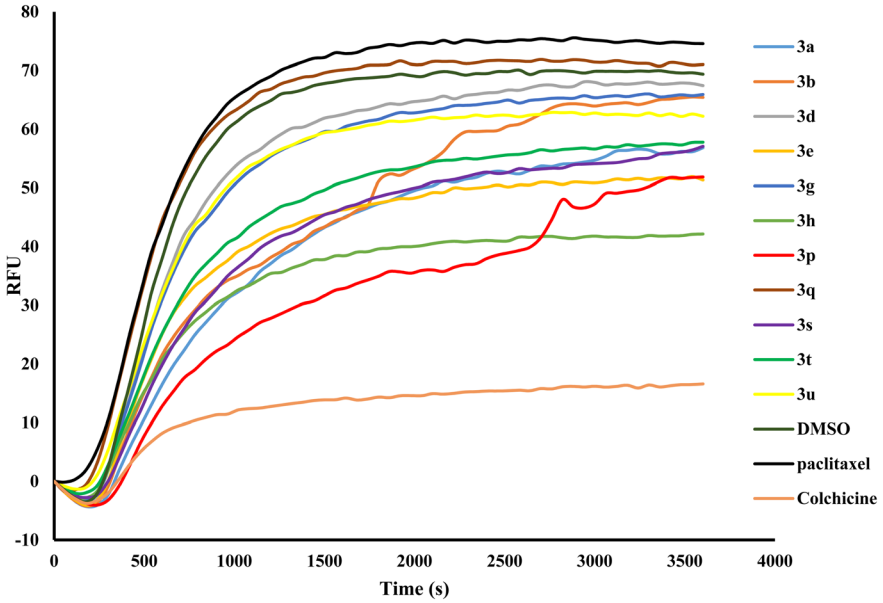

Fig. 3 Effects of derivatives **3a–b**, **3d–e**, **3g–h**, **3p–q**, and **3s–u** at a concentration of 10 μM on tubulin polymerization assay at 37 °C with colchicine (10 μM) as appositive control and paclitaxel (3 μM) as negative control. The curve is the average from two experiment runs.

micromolar values. However, aromatase inhibitory activities of the derivatives lacked correlation with anti-breast cancer activities suggesting that the series can act on multiple pathways. The strongest aromatase inhibitor was the ester derivative, **3k** (IC_{50} = 18 nM), which has a strong electron-withdrawing ester group at position X_4. Unfortunately, **3k** has relatively moderate growth inhibition activities, and hence, the GI_{50} values of **3k** were not determined by NCI. In this regard, the IC_{50} values were determined for the derivatives against the T47D breast cancer cell line based on our protocol. Initially, the derivatives were screened at two different concentrations, 10 μM and 50 μM respectively (Fig. S4†). Most of the derivatives displayed promising results from the two-dose experimental. However, alternate pyrrole (**3b**), derivatives with carboxylic acid substituents (**3l–m** and **3w**), nitro group (**3p–q**), amide group (**3x**) showed weak activity. Promising candidates were evaluated for cytotoxic activity with T47D. The determined GI_{50} and IC_{50} values have relatively satisfactory correlations with R^2 = 0.788 suggesting the results are relatively reliable (Fig. S5†). From this, it was revealed that **3k** showed relatively moderate antiproliferative effects against T47D with IC_{50} = 10.6 μM. From Table 2, aromatase inhibition tends to be stronger with electron-withdrawing groups at positions X_3 and X_4 on the pyrrole ring for the 2-pyrrolyl derivatives, so only **3v** (IC_{50} = 2.5 μM) and **3x** (IC_{50} = 3.7 μM) in the 3-pyrrolyl derivatives were active. The trisubstituted derivative, **3r** (IC_{50} = 0.2 μM) was the second best aromatase inhibitor, followed by **3f**, **3j**, **3h** and **3o**, which contain electron-withdrawing groups at X_3 with IC_{50} values ranging between 1.3 to 1.8 μM, whereas **3a**, **3g**, **3i**, **3n** and **3v** were slightly less potent with IC_{50} values ranging between 2.5 to 3.4 μM. Single bromo-substituted derivative **3e**, and ethyl-substituted derivatives **3s** and **3t** exhibited weaker IC_{50} values between 4.0 to 4.7 μM, whilst **3c** and **3u** which contain electron-donating alkyl groups at X_4 are weaker inhibitors with IC_{50} values at 11.1 and 9.7 μM, respectively. Despite the fact that *N*-methylation of pyrrole (**3d**) showed inactivity against aromatase, it exhibited the most potent antiproliferative effects for T47D (IC_{50} = 1.0 μM), comparable to **3a** (IC_{50} = 1.6 μM). The carboxylated derivatives **3l**, **3m**, and **3w**, and single nitro-substituted derivative **3q** were inactive against aromatase. The unsubstituted furanyl- (**1a**) and thiophenyl- (**2a**) derivatives were also tested for aromatase inhibition. Interestingly, furanyl **1a** was able to inhibit aromatase, albeit with weak potency (IC_{50} = 11.3 μM). However, thiophenyl **2a** lacked aromatase inhibition.

2.2.5. *In vitro* toxicity in non-tumoral cell line. To determine the toxic effects of the derivatives in a non-tumour cell line, the cytotoxic effects of the derivatives were tested against the L929 normal mouse fibroblast cell line and compared to the T47D cell line (Table 2). Derivatives **3d**, **3i** and **3r** were determined to have no toxicity towards L929 cells at 50 μM single concentration, *i.e.*, >80% cell survival. The IC_{50} values were determined for other derivatives with <80% L929 cell survival tested at 50 μM single concentration. Interestingly, the highly potent single halogen-substituted derivatives **3e** and **3h** were some of the least toxic derivatives with SI ∼ 22 for **3h** and SI ∼ 9 for **3e**, followed by the non-substituted parent compound, **3a** (SI ∼ 16). Derivatives **3s**, **3n**, **3v** and **3o**, had SI values in the range of 3.5 and 5.1. Derivatives **3c**, **3f**, **3g** and **3u** displayed approximately two-folds less toxicity against normal cell line L929 than in T47D cancer cells, whilst **3j**, **3k** and **3t** exhibited relatively similar toxicity profiles in both cell lines.

2.3. Molecular modelling

2.3.1. Molecular docking analysis of derivatives to tubulin. From the literature, it is known that compounds with the 3-phenyl-1*H*-indole-2-carbohydrazide core scaffold interact most

Open Access Article. Published on 27 June 2025. Downloaded on 12/13/2025 6:15:48 PM.
This article is licensed under a Creative Commons Attribution 3.0 Unported Licence.

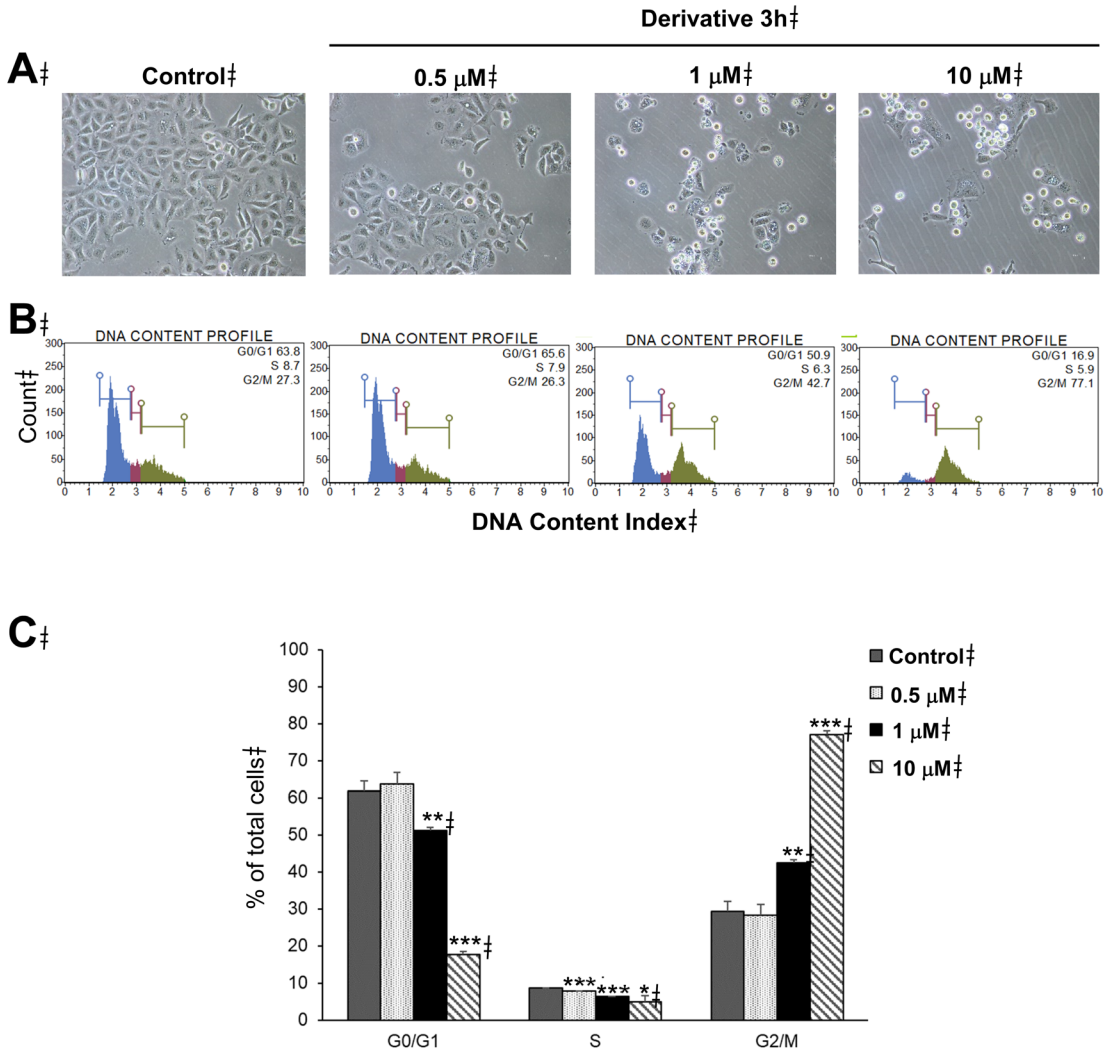

Fig. 4 Effects of derivative **3h** on cell morphology and cell cycle progression of A549 human non-small cell lung cancer cells. The cells were treated with **3h** at indicated concentrations for 24 h. The cells were subjected to cell cycle analysis by flow cytometric method. (A) Cell morphology after treatment, images of a representative experiment are shown with original magnification of ×200. (B) DNA content histograms of a representative experiment. (C) Percentages of cell populations in G0/G1, S, and G2/M phases. Data are shown as average with SD from three independent experiments, *$p < 0.05$, **$p < 0.01$, and ***$p < 0.001$ *versus* control group.

favorably with the colchicine binding site located at the α- and β-subunit interface leading to destabilization of the microtubule structure.[27–29] Thus, we planned to dock the pyrrolyl derivatives into the colchicine site of tubulin to study their mechanism of binding. However, before this was performed, the docking protocol was first validated by docking the co-crystallized structure of colchicine to the colchicine binding site of tubulin in accordance with the protocol (see Experimental section 4.7). The docked conformation of colchicine was overlaid on to the co-crystallized structure (Fig. S6†) and the root-mean square deviation (RMSD) was calculated to be 1.33 Å using the DockRMSD[34] web server as previous described[28] suggesting the reproducibility of the results and reliability of the docking procedures, *i.e.*, RMSD < 2 Å.[35] Following this, the derivatives were docked to the colchicine binding site of tubulin. The binding mode of the pyrrolyl series can be exemplified by the most active derivative **3h** as shown in Fig. 5. The pyrrolyl derivatives were predicted to have a different binding orientation to the furanyl and thiophenyl derivatives, which can explain their weaker tubulin inhibitory activities. Interactions between the pyrrolyl derivatives and the colchicine site lacked hydrogen bonding and tended to rely mainly on hydrophobic and dipole–dipole interactions. Orientation of the pyrrolyl side chain tend to reside with the β-subunit of tubulin with dipole–dipole interactions seen with Asn249. The 3-phenyl-1*H*-indole-2-carbohydrazide core scaffold is predicted to form hydrophobic interactions with vicinal hydrophobic residues Leu248, Ala250, Leu255, Ala316 and Ile318 in the hydrophobic region of the colchicine site.

2.3.2. Molecular docking analysis of derivatives to aromatase. To elucidate the mechanism of the binding of pyrrolyl derivatives to aromatase, the derivatives were docked to the binding site of aromatase. The docking protocol was validated by docking the co-crystallized structure of exemestane to the

© 2025 The Author(s). Published by the Royal Society of Chemistry

Open Access Article. Published on 27 June 2025. Downloaded on 12/13/2025 6:15:48 PM. This article is licensed under a Creative Commons Attribution 3.0 Unported Licence.

Table 2 The aromatase inhibition, antiproliferative activities and *in vitro* toxicity data of derivatives **1a**, **2a**, and **3a–x**, expressed as IC_{50} values (μM)

Derivative	Aromatase (μM)	T47D[a] (μM)	L929[a] (μM)	Selectivity index[d] (SI)
1a	11.3 ± 1.7	—[b]	—[b]	—
2a	>12.5	—[b]	—[b]	—
3a	3.4 ± 0.6	1.6 ± 1.0	26.3 ± 14.5	16.4
3b	11.0 ± 1.3	—[b]	—[b]	—
3c	11.1 ± 2.0	11.6 ± 0.3	29.5 ± 12.6	2.54
3d	>12.5	1.0 ± 0.4	—[c]	—
3e	4.0 ± 1.0	2.4 ± 1.4	22.3 ± 11.9	9.29
3f	1.5 ± 0.3	19.1 ± 5.4	47.9 ± 0.5	2.51
3g	2.6 ± 0.5	8.2 ± 1.8	20.1 ± 10.3	2.45
3h	1.8 ± 0.4	2.4 ± 1.8	53.7 ± 30.4	22.4
3i	2.6 ± 0.8	11.8 ± 1.4	—[c]	—
3j	1.3 ± 0.4	10.4 ± 2.9	12.2 ± 1.0	1.17
3k	0.018 ± 0.002	10.6 ± 1.1	15.0 ± 8.9	1.42
3l	>12.5	—[b]	—[b]	—
3m	>12.5	—[b]	—[b]	—
3n	3.3 ± 0.6	5.4 ± 4.8	21.8 ± 11.5	4.04
3o	1.6 ± 0.4	14.9 ± 1.0	43.2 ± 9.9	3.57
3p	1.4 ± 0.3	—[b]	—[b]	—
3q	>12.5	—[b]	—[b]	—
3r	0.2 ± 0.1	12.3 ± 0.3	—[c]	—
3s	4.6 ± 0.5	3.8 ± 1.0	19.5 ± 11.8	5.13
3t	4.7 ± 0.5	4.6 ± 2.9	7.1 ± 3.6	1.54
3u	9.6 ± 1.0	6.2 ± 3.6	12.2 ± 0.7	1.97
3v	2.5 ± 0.6	24.9 ± 8.4	90.1 ± 40.3	3.62
3w	>12.5	—[b]	—[b]	—
3x	3.7 ± 0.6	—[b]	—[b]	—
Letrozole	0.0014 ± 0.0003	—[b]	—[b]	—
Cisplatin	—[b]	>100	23.7 ± 8.9	—

[a] IC_{50} values determined by protocol in Methodology section 4.6. [b] Not determined. [c] No toxicity observed at 50 μM single concentration (>80% cell survival). [d] = IC_{50} (L929)/IC_{50} (T47D).

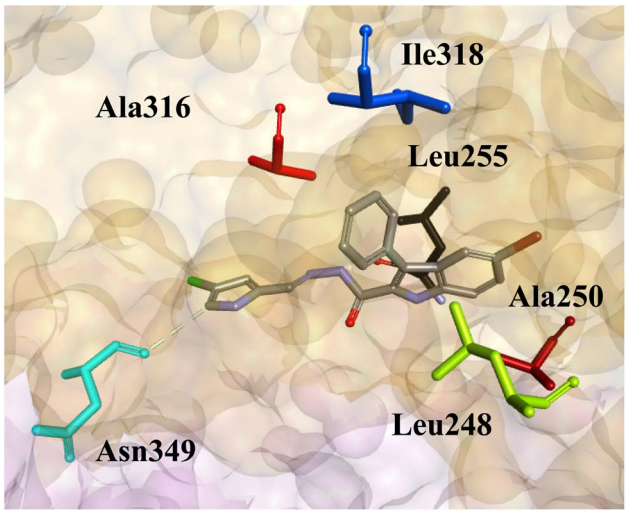

Fig. 5 The predicted binding orientation of derivative **3h** at the colchicine binding site. The dipole–dipole interactions between Asn349 and the ligands are shown. The surface of tubulin was rendered orange for the β-subunit and light pink for the α-subunit. Amino acid residues Ala316, Ile318, Leu255, Ala250, Leu248 and Asn349 are depicted as sticks and colored as red, blue, black, brown, lime green and turquoise, respectively.

aromatase binding site in accordance to the protocol in the Experimental section 4.7. The docked conformation of exemestane was overlaid to the co-crystallized structure (Fig. S7†) and the root-mean squared deviation (RMSD) was calculated to be 0.46 Å using the DockRMSD[34] web server, which suggest the reliability of the docking protocol and reproducibility of the docking results.[35] The binding modes of the pyrrolyl derivatives are represented by the most active derivative **3k** (Fig. 6). It can be seen that the hydrazone functionality and the pyrrole ring is oriented towards the heme group, and is predicted to chelate with heme iron, which can explain the lack of inhibition by non-chelating entities, *e.g.*, thiophenyl **2a** and *N*-methylated pyrrole **3d**. However, furanyl **1a** exhibited inhibition of aromatase suggesting the hydrazone potentially holds a fair share of influence over heme chelation for some derivatives. Inhibition of the series to aromatase is predicted to be accommodated mainly by hydrophobic interactions with surrounding hydrophobic residues, with the phenyl group is oriented to nearby Trp224, Tyr220, Phen221 and Ile305, the indole scaffold is oriented to form interactions with Phe134, Ile70, Met374 and Leu372, whereas the pyrrole ring is predicted to interact with Val369.

2.3.3. Chemical space. The physicochemical properties of the new derivatives were predicted using the Dragon 7.0 software. The software calculates for the molecular descriptors that are generally used to assess the pharmacokinetic profiles of drugs: molecular weight (MW), hydrogen bond donors (HD) and acceptors (HA), rotatable bonds (RB), Moriguchi log P (*M*logP)[36] and polar surface area (PSA). The results are shown in Table S8.†

Open Access Article. Published on 27 June 2025. Downloaded on 12/13/2025 6:15:48 PM. This article is licensed under a Creative Commons Attribution 3.0 Unported Licence.

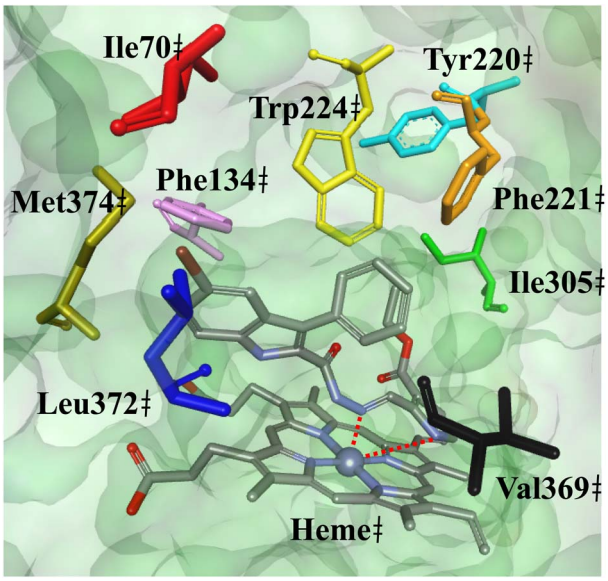

Fig. 6 The predicted binding orientation of derivative **3k** in the aromatase binding site. Potential chelation between **3k** and heme (blue spherical shape) is depicted as red dotted lines. The surface of the aromatase was rendered in green. Amino acid residues Ile70, Phe134, Tyr220, Phe221, Trp224, Val369, Ile305, Leu372, and Met374 are depicted in sticks and colored as red, turquoise, orange, yellow, black, green, blue, and olive green, respectively.

Results revealed that most synthesized derivatives are within the Lipinski's[37] and Veber's[38] limits, *i.e.*, most derivatives are predicted to be adequate for oral drug administration. Nonetheless, derivatives with dibromo (**3f**) and morpholine-4-carbonyl (**3n**, **3o** and **3x**) substitutions are large in size resulting in the molecular weights exceeding the 500 g mol^{-1} Lipinski's limit.

The toxicity profiles of the most active compounds were predicted using ADMETlab 3.0.[39] The results of the mainstream toxicity types for the compounds are shown in Table S9.† The compounds were predicted to have low cardiotoxic and immunotoxic effects with moderate chances of being mutagens, albeit they are generally well-tolerated. Nonetheless, strong heptotoxic effects were predicted, which indicate further need for hepatotoxicity studies.

3. Conclusion

In this study, twenty-four new pyrrolyl-3-phenyl-1*H*-indole-2-carbohydrazides were successfully designed, synthesized and evaluated for their dual inhibitory effects against two targets: tubulin and aromatase. Derivative **3h** which has a single chloro substitution at X_3 was the strongest tubulin inhibitor with strong aromatase inhibitory activity. Furthermore, strong lethal effects and growth inhibition activities were observed for **3h**, which was confirmed to cause mitotic arrest at the G2/M phase. Ester derivative **3k** was the best aromatase inhibitor but exhibited moderate antiproliferative effects. In general, electron-withdrawing substituents tended to favor aromatase inhibition. However, the series lacked correlation between aromatase inhibition and anti-T47D breast cancer activities. All derivatives displayed lower cytotoxic effects against the non-tumoral L929 cell line compared to the T47D cancer cell line. Molecular docking predicted the subseries interact with and inhibit tubulin at the colchicine site and revealed that in addition to the pyrrole as a chelating group, the hydrazone functionality is predicted to contribute to heme chelation for some derivatives resulting in the subsequent inhibition of aromatase. Eight cancer cell lines were particularly sensitive to the subseries: HL-60 (TB), COLO 205, LOX IMVI, MDA-MB-435, SK-MEL-5, OVCAR-8, NCI/(ADR-RES) and SN12C. Strong antiproliferative effects against COLO 205, MDA-MB-435, SK-MEL-5 and OVCAR-8 cancer cell lines are shared with precedent furanyl and thiophenyl subseries. The derivatives were mostly predicted to be drug-like with acceptable oral pharmacokinetics. The most active compounds were generally predicted to have adequate toxicity profiles, aside from speculation of strong hepatotoxic effects.

4. Experimental section

4.1. Synthesis

All chemicals for synthesis were purchased from commercial suppliers and used directly unless specifically stated. Thin layer chromatography was performed on Merck silica gel 60 F254 plates and visualized by UV irradiation at 254 nm. Flash column chromatography was performed using SilicaFlash® F60 (40–63 μm) or (63–200 μm) to obtain purified products. Automated flash chromatography was performed on Ultra Performance Flash Purification Chromatography (Model: Interchim puriflash 5.050) to obtain purified products. Bruker AVANCE-400 and 600 MHz were used to collect ^{1}H and ^{13}C NMR spectra. Chemical shifts (δ) are reported in parts-per-million (ppm) with respect to the solvent peaks and coupling constants (J) are in Hertz. Multiplicity of NMR peaks are given the abbreviations: s = singlet, d = doublet, t = triplet, q = quartet, m = multiplet, br = broad. Thermo Scientific Nicolet iS 5 Fourier Transform IR spectrometer was used to record Infrared (IR) spectra. Only selected peaks are reported and absorption maxima are given in cm^{-1}. Thermo Scientific Orbitrap Q Exactive Focus mass spectrometer was used to record High Resolution mass spectra (HR-MS). Melting points were measured by using a Stuart SMP30 capillary melting point apparatus.

4.1.1. 5-Bromo-3-phenyl-1*H*-indole-2-carbohydrazide (5). To a solution of indole **5** (0.864 g, 2.59 mmol) in EtOH (30 mL), was added hydrazine (50% in H_2O, 9.60 mL, 154.11 mmol). The resulting mixture was cooled to room temperature, and the solvent was evaporated. Solid product was recrystallized from EtOH giving 5-bromo-3-phenyl-1*H*-indole-2-carbohydrazide **5** (0.610 g, 1.85 mmol, 71%) as a pale yellow solid; mp 240–242 °C, lit.[25] mp for **5** 242–244 °C; ^{1}H NMR (400 MHz, $(CD_3)_2SO$) δ 11.94 (s, 1H), 8.89 (s, 1H), 7.62 (d, J = 1.8 Hz, 1H), 7.49–7.35 (m, 7H), 4.49 (s, 1H). The data were consistent with that in the literature.[25]

4.1.2. (*E*)-*N*′-((1*H*-Pyrrol-2-yl)methylene)-5-bromo-3-phenyl-1*H*-indole-2-carbohydrazide (3a). To a solution of hydrazide **2** (0.071 g, 0.22 mmol) in EtOH (10 mL) was added pyrrole-2-

© 2025 The Author(s). Published by the Royal Society of Chemistry

Open Access Article. Published on 27 June 2025. Downloaded on 12/13/2025 6:15:48 PM. This article is licensed under a Creative Commons Attribution 3.0 Unported Licence.

carboxaldehyde (0.021 g, 0.22 mmol) and a few drop of acetic acid. The resulting mixture was heated to 80 °C, and stirred for 17 h. The reaction mixture was allowed to cool to room temperature, and solvent was evaporated. Purification by flash column chromatography, eluted with EtOAc–hexane (1 : 9 to 1 : 1), gave indole hydrazide **3a** (0.085 g, 0.21 mmol, 95%) as a yellow solid; R_f 0.5 [EtOAc–hexane (1 : 1)]; mp 206 °C decomposed; ^{1}H NMR (600 MHz $(CD_3)_2SO$) δ 12.14 (s, 1H), 11.51 (s, 1H), 11.07 (s, 1H), 7.87 (s, 1H), 7.71 (s, 1H), 7.50–7.44 (m, 5H), 7.38 (dd, J = 8.6, 1.9 Hz, 1H), 7.34 (t, J = 7.5 Hz, 1H), 6.89 (s, 1H), 6.42 (s, 1H), 6.10 (s, 1H); ^{13}C NMR (150 MHz $(CD_3)_2SO$) δ 157.66, 140.54, 134.29, 133.10, 129.53, 129.28, 128.58, 127.88, 126.85, 126.75, 126.34, 122.78, 121.83, 116.76, 114.47, 113.62, 112.91, 109.40; ν_{max}/cm^{-1} 3254, 1629, 1599, 1290; HRMS (ESI) m/z [M + H]$^+$ calcd for $C_{20}H_{16}ON_4{}^{79}Br$ 407.0502; found 407.0504. Compounds **3e**, **3g**, **3f** and **3h** were synthesized following the procedure described here.

4.1.3. (*E*)-5-Bromo-*N*′-((4-bromo-1*H*-pyrrol-2-yl)methylene)-3-phenyl-1*H*-indole-2-carbohydrazide (3e). Yellow solid (0.103 g, 0.21 mmol, 95%); R_f 0.6 [EtOAc–hexane (1 : 1)]; mp 231–233 °C decomposed; ^{1}H NMR (600 MHz $(CD_3)_2SO$) δ 12.05 (s, 1H), 11.76 (s, 1H), 11.15 (s, 1H), 7.76 (s, 1H), 7.62 (s, 1H), 7.41–7.35 (m, 5H), 7.30–7.23 (m, 2H), 6.91 (s, 1H), 6.44 (s, 1H); ^{13}C NMR (150 MHz $(CD_3)_2SO$) δ 157.98, 139.39, 134.40, 133.07, 129.62, 129.01, 128.66, 127.94, 127.87, 126.98, 126.55, 122.31, 121.95, 117.19, 114.58, 114.35, 113.04, 96.05; ν_{max}/cm^{-1} 3305, 1645, 1615, 1538, 1288; HRMS (ESI) m/z [M + H]$^+$ calcd for $C_{20}H_{15}ON_4{}^{79}Br_2$ 484.9607; found 484.9604.

4.1.4. (*E*)-5-Bromo-*N*′-((4,5-dibromo-1*H*-pyrrol-2-yl)methylene)-3-phenyl-1*H*-indole-2-carbohydrazide (3f). Yellow solid (0.145 g, 0.26 mmol, 96%); R_f 0.5 [EtOAc–hexane (2 : 3)]; mp 164 °C decomposed; ^{1}H NMR (600 MHz $(CD_3)_2SO$) δ 12.64 (s, 1H), 12.08 (s, 1H), 11.23 (s, 1H), 7.73 (s, 1H), 7.64 (s, 1H), 7.42–7.26 (m, 7H), 6.56 (s, 1H); ^{13}C NMR (150 MHz $(CD_3)_2SO$) δ 158.03, 138.69, 134.39, 133.03, 129.60, 129.13, 128.89, 128.63, 127.91, 126.97, 126.57, 121.95, 117.28, 115.11, 114.57, 113.04, 105.49, 99.00; ν_{max}/cm^{-1} 3259, 3066, 1646, 1536, 1244; HRMS (ESI) m/z [M + H]$^+$ calcd for $C_{20}H_{14}ON_4{}^{79}Br_3$ 562.8712; found 562.8714.

4.1.5. (*E*)-5-Bromo-*N*′-((3-chloro-1*H*-pyrrol-2-yl)methylene)-3-phenyl-1*H*-indole-2-carbohydrazide (3g). Yellow solid (0.105 g, 0.24 mmol, quantitative); R_f 0.7 [EtOAc–hexane (1 : 1)]; mp 170 °C decomposed; ^{1}H NMR (400 MHz $(CD_3)_2SO$) δ 12.34 (s, 1H), 12.17 (s, 1H), 11.18 (s, 1H), 7.84 (s, 1H), 7.74 (s, 1H), 7.54–7.36 (m, 7H), 6.47 (s, 1H), 6.11 (s, 1H); ^{13}C NMR (100 MHz $(CD_3)_2SO$) δ 157.83, 139.78, 134.34, 133.07, 129.56, 129.11, 128.60, 127.91, 126.91, 126.77, 126.44, 121.88, 118.52, 116.99, 114.53, 114.18, 112.96, 107.96; ν_{max}/cm^{-1} 3241, 3080, 1645, 1538, 1246; HRMS (ESI) m/z [M + H]$^+$ calcd for $C_{20}H_{15}ON_4{}^{79}Br^{35}Cl$ 441.0112; found 441.0112.

4.1.6. (*E*)-5-Bromo-*N*′-((4-chloro-1*H*-pyrrol-2-yl)methylene)-3-phenyl-1*H*-indole-2-carbohydrazide (3h). Yellow solid (0.039 g, 0.09 mmol, 38%); R_f 0.6 [EtOAc–hexane (1 : 1)]; mp 190 °C decomposed; ^{1}H NMR (400 MHz $(CD_3)_2SO$) δ 12.14 (s, 1H), 11.78 (s, 1H), 11.22 (s, 1H), 7.84 (s, 1H), 7.71 (s, 1H), 7.51–7.33 (m, 7H), 6.97 (s, 1H), 6.48 (s, 1H); ^{13}C NMR (100 MHz $(CD_3)_2SO$) δ 157.81, 139.51, 134.30, 133.02, 129.52, 129.02, 128.55, 127.84, 126.86, 126.41, 121.85, 119.76, 117.01, 114.49, 112.92, 111.73, 111.57; ν_{max}/cm^{-1} 3254, 1613, 1537, 1237; HRMS (ESI) m/z [M + H]$^+$ calcd for $C_{20}H_{15}ON_4{}^{79}Br^{35}Cl$ 441.0112; found 441.0113.

4.1.7. (*E*)-*N*′-((1*H*-Pyrrol-3-yl)methylene)-5-bromo-3-phenyl-1*H*-indole-2-carbohydrazide (3b). To a solution of hydrazide **2** (0.091 g, 0.28 mmol) in EtOH (10 mL) was added pyrrole-3-carboxaldehyde (0.027 g, 0.28 mmol) and a few drops of acetic acid. The resulting mixture was heated to 80 °C, and stirred for 17 h. The reaction mixture was allowed to cool to room temperature, and solvent was evaporated. Purification by automated flash chromatography, eluted with EtOAc–hexane (0 : 100 to 100 : 0), gave indole hydrazide **3b** (0.096 g, 0.24 mmol, 86%) as a brown solid; R_f 0.5 [EtOAc–hexane (100 : 0)]; mp 177–180 °C decomposed; ^{1}H NMR (600 MHz $(CD_3)_2SO$) δ 12.09 (s, 1H), 11.15 (s, 1H), 10.88 (s, 1H), 7.90 (s, 1H), 7.69 (s, 1H), 7.50–7.44 (m, 5H), 7.37–7.33 (m, 2H), 7.15 (s, 1H), 6.80 (s, 1H), 6.36 (s, 1H); ^{13}C NMR (150 MHz $(CD_3)_2SO$) δ 157.48, 144.53, 134.22, 133.15, 129.57, 129.42, 128.57, 127.96, 126.83, 126.25, 122.01, 121.78, 120.10, 119.01, 116.61, 114.44, 112.85, 105.30; ν_{max}/cm^{-1} 3239, 3049, 1629, 1557, 1288; HRMS (ESI) m/z [M + H]$^+$ calcd for $C_{20}H_{16}ON_4{}^{79}Br$ 407.0502; found 407.0495. Compounds **3k**, **3o** (eluted with MeOH–CH_2Cl_2 (0 : 100 to 15 : 85)), and **3s–u** were synthesized following the procedure described here.

4.1.8. Ethyl (*E*)-2-((2-(5-bromo-3-phenyl-1*H*-indole-2-carbonyl)hydrazono)methyl)-1*H*-pyrrole-3-carboxylate (3k). Yellow solid (0.097 g, 0.20 mmol, 83%); R_f 0.4 [EtOAc–hexane (1 : 1)]; mp 259–261 °C decomposed; ^{1}H NMR (600 MHz $(CD_3)_2SO$) δ 12.16 (s, 1H), 12.04 (s, 1H), 11.54 (s, 1H), 8.59 (s, 1H), 7.72 (s, 1H), 7.51–7.33 (m, 7H), 6.86 (s, 1H), 6.47 (s, 1H), 4.18 (q, J = 7.1 Hz, 2H), 1.24 (t, J = 7.1 Hz, 3H); ^{13}C NMR (150 MHz $(CD_3)_2SO$) δ 163.79, 158.06, 139.50, 134.35, 133.07, 129.94, 129.56, 128.86, 128.56, 127.87, 126.88, 126.51, 122.15, 121.91, 117.33, 116.43, 114.53, 112.97, 111.09, 59.51, 14.35; ν_{max}/cm^{-1} 3262, 3061, 2853, 1698, 1640, 1538, 1268; HRMS (ESI) m/z [M + H]$^+$ calcd for $C_{23}H_{20}O_3N_4{}^{79}Br$ 479.0713; found 479.0712.

4.1.9. (*E*)-5-Bromo-*N*′-((4-(morpholine-4-carbonyl)-1*H*-pyrrol-2-yl)methylene)-3-phenyl-1*H*-indole-2-carbohydrazide (3o). Yellow solid (0.09 g, 0.17 mmol, 94%); R_f 0.5 [MeOH–CH_2Cl_2 (7 : 93)]; mp 198–200 °C; ^{1}H NMR (600 MHz $(CD_3)_2SO$) δ 12.15 (s, 1H), 11.94 (s, 1H), 11.23 (s, 1H), 7.90 (s, 1H), 7.71 (s, 1H), 7.51–7.44 (m, 5H), 7.38 (dd, J = 8.6, 1.9 Hz, 1H), 7.34 (t, J = 7.4 Hz, 1H), 7.20 (s, 1H), 6.64 (s, 1H), 3.57 (s, 8H); ^{13}C NMR (150 MHz $(CD_3)_2SO$) δ 164.66, 157.82, 139.89, 134.33, 133.04, 129.53, 129.07, 128.58, 127.86, 127.00, 126.88, 126.43, 125.09, 121.87, 119.01, 116.98, 114.50, 113.61, 112.95, 66.27; ν_{max}/cm^{-1} 3213, 2856, 1601, 1544, 1225; HRMS (ESI) m/z [M + H]$^+$ calcd for $C_{25}H_{23}O_3N_5{}^{79}Br$ 520.0979; found 520.0977.

4.1.10. (*E*)-5-Bromo-*N*′-((5-ethyl-1*H*-pyrrol-2-yl)methylene)-3-phenyl-1*H*-indole-2-carbohydrazide (3s). Yellow solid (0.110 g, 0.25 mmol, 96%); R_f 0.5 [EtOAc–hexane (1 : 1)]; mp 136 °C decomposed; ^{1}H NMR (600 MHz $(CD_3)_2SO$) δ 12.08 (s, 1H), 11.23 (s, 1H), 10.93 (s, 1H), 7.72 (s, 1H), 7.66 (s, 1H), 7.45–7.39 (m, 5H), 7.33 (dd, J = 8.7, 1.9 Hz, 1H), 7.29 (t, J = 7.4 Hz, 1H), 6.25 (s, 1H), 5.79 (s, 1H), 2.52 (q, J = 7.6 Hz, 2H), 1.10 (t, J = 7.6 Hz, 3H); ^{13}C NMR (150 MHz $(CD_3)_2SO$) δ 157.59, 140.63, 139.96, 134.32, 133.16, 129.55, 129.42, 128.62, 127.94, 126.89, 126.33, 125.49,

Open Access Article. Published on 27 June 2025. Downloaded on 12/13/2025 6:15:48 PM. This article is licensed under a Creative Commons Attribution 3.0 Unported Licence.

121.84, 116.67, 114.66, 114.49, 112.94, 106.43, 20.41, 13.96; ν_{max}/cm^{-1} 3313, 2925, 1612, 1544, 1247; HRMS (ESI) m/z [M + H]$^+$ calcd for $C_{22}H_{20}ON_4{}^{79}Br$ 435.0815; found 435.0812.

4.1.11. (*E*)-5-Bromo-*N*′-((4-ethyl-1*H*-pyrrol-2-yl)methylene)-3-phenyl-1*H*-indole-2-carbohydrazide (3t). Yellow solid (0.095 g, 0.22 mmol, 88%); R_f 0.5 [EtOAc–hexane (1 : 1)]; mp 141 °C decomposed; ^{1}H NMR (600 MHz $(CD_3)_2SO$) δ 12.08 (s, 1H), 11.13 (s, 1H), 10.98 (s, 1H), 7.75 (s, 1H), 7.66 (s, 1H), 7.45–7.38 (m, 5H), 7.32 (dd, J = 8.6, 1.9 Hz, 1H), 7.29 (t, J = 7.4 Hz, 1H), 6.63 (s, 1H), 6.24 (s, 1H), 2.34 (q, J = 7.6 Hz, 2H), 1.05 (t, J = 7.5 Hz, 3H); ^{13}C NMR (150 MHz $(CD_3)_2SO$) δ 157.65, 140.57, 134.33, 133.14, 129.58, 129.32, 128.62, 127.94, 126.89, 126.57, 126.51, 126.37, 121.87, 119.93, 116.81, 114.50, 113.15, 112.95, 19.49, 15.36; ν_{max}/cm^{-1} 3313, 2928, 1613, 1544, 1247; HRMS (ESI) m/z [M + H]$^+$ calcd for $C_{22}H_{20}ON_4{}^{79}Br$ 435.0815; found 435.0812.

4.1.12. (*E*)-5-Bromo-*N*′-((3-ethyl-1*H*-pyrrol-2-yl)methylene)-3-phenyl-1*H*-indole-2-carbohydrazide (3u). Yellow solid (0.106 g, 0.24 mmol, 92%); R_f 0.5 [EtOAc–hexane (1 : 1)]; mp 154 °C decomposed; ^{1}H NMR (600 MHz $(CD_3)_2SO$) δ 12.09 (s, 1H), 11.17 (s, 1H), 10.96 (s, 1H), 7.95 (s, 1H), 7.68 (s, 1H), 7.48–7.41 (m, 5H), 7.34 (dd, J = 8.6, 1.9 Hz, 1H), 7.31 (t, J = 7.4 Hz, 1H), 6.76 (s, 1H), 5.95 (s, 1H), 2.43 (q, J = 7.5 Hz, 2H), 1.06 (t, J = 7.6 Hz, 3H); ^{13}C NMR (150 MHz $(CD_3)_2SO$) δ 157.47, 139.53, 134.30, 133.17, 130.74, 129.59, 129.39, 128.59, 127.93, 126.82, 126.34, 122.29, 122.25, 121.85, 116.76, 114.47, 112.93, 109.21, 18.54, 16.03; ν_{max}/cm^{-1} 3312, 3058, 2925, 1606, 1538, 1248; HRMS (ESI) m/z [M + H]$^+$ calcd for $C_{22}H_{20}ON_4{}^{79}Br$ 435.0815; found 435.0811.

4.1.13. (*E*)-5-Bromo-*N*′-((3,5-dimethyl-1*H*-pyrrol-2-yl)methylene)-3-phenyl-1*H*-2-carbohydrazide (3c). To a solution of hydrazide **2** (0.081 g, 0.25 mmol) in EtOH (10 mL) was added 3,5-dimethyl-2-pyrrolecarboxaldehyde (0.031 g, 0.25 mmol) and a few drops of acetic acid. The resulting mixture was heated to 80 °C, and stirred for 17 h. The reaction mixture was allowed to cool to room temperature. Precipitated solid was filtered, and was washed with EtOH (10 mL) to give indole hydrazide **3c** (0.073 g, 0.17 mmol, 68%) as a yellow solid; mp 153–155 °C decomposed; ^{1}H NMR (600 MHz $(CD_3)_2SO$) δ 11.96 (s, 1H), 10.82 (s, 1H), 10.78 (s, 1H), 7.72 (s, 1H), 7.57 (s, 1H), 7.36–7.30 (m, 5H), 7.24 (dd, J = 8.7, 1.9 Hz, 1H), 7.21 (t, J = 7.2 Hz, 1H), 5.52 (s, 1H), 2.00 (s, 3H), 1.84 (s, 3H); ^{13}C NMR (150 MHz $(CD_3)_2SO$) δ 157.52, 139.35, 134.39, 133.28, 133.00, 129.66, 129.53, 128.72, 128.04, 126.96, 126.40, 124.78, 121.96, 121.60, 116.73, 114.57, 113.01, 109.92, 12.84, 10.83; ν_{max}/cm^{-1} 3312, 3058, 2863, 1610, 1545, 1241; HRMS (ESI) m/z [M + H]$^+$ calcd for $C_{22}H_{20}ON_4{}^{79}Br$ 435.0815; found 435.0809. Compounds **3d**, **3i–j**, **3l–n**, **3p–r** and **3v–x** were synthesized following the procedure described here.

4.1.14. (*E*)-5-Bromo-*N*′-((1-methyl-1*H*-pyrrol-2-yl)methylene)-3-phenyl-1*H*-indole-2-carbohydrazide (3d). Brown solid (0.052 g, 0.12 mmol, 57%); mp 261 °C decomposed; ^{1}H NMR (600 MHz $(CD_3)_2SO$) δ 8.01 (s, 1H), 7.87 (s, 0.3H)*, 7.75 (s, 0.3H)*, 7.71 (s, 1H), 7.54–7.34 (m, 7H), 7.25 (s, 0.3H), 6.97 (s, 1H), 6.79 (s, 0.3H)*, 6.46 (s, 1H), 6.30 (s, 0.3H)*, 6.09 (s, 1H), 5.99 (s, 0.3H)*, 3.84 (s, 3H); ^{13}C NMR (100 MHz $(CD_3)_2SO$) δ 157.57, 140.67, 134.25, 133.08, 129.62, 129.14, 128.52, 128.33, 127.98, 126.83, 126.76, 126.38, 121.84, 117.05, 114.96, 114.47, 112.90, 108.46, 35.94; ν_{max}/cm^{-1} 3262, 3051, 1649, 1535, 1236; HRMS (ESI) m/z [M + H]$^+$ calcd for $C_{21}H_{18}ON_4{}^{79}Br$ 421.0659; found 421.0655.

* Rotamer.

^{1}H NMR (600 MHz $(CD_3)_2SO$, 90 °C) δ 7.99 (s, 1H), 7.69 (d, J = 1.9 Hz, 1H), 7.54–7.53 (m, 2H), 7.48–7.46 (m, 3H), 7.37–7.34 (m, 2H), 6.89 (s, 1H), 6.41 (s, 1H), 6.07 (s, 1H), 3.74 (s, 3H).

4.1.15. Ethyl (*E*)-5-((2-(5-bromo-3-phenyl-1*H*-indole-2-carbonyl)hydrazono)methyl)-1*H*-pyrrole-2-carboxylate (3i). Yellow solid (0.114 g, 0.24 mmol, 96%); mp 247–249 °C; ^{1}H NMR (600 MHz $(CD_3)_2SO$) δ 12.36 (s, 1H), 12.16 (s, 1H), 11.95 (s, 0.3H)*, 11.89 (s, 0.3H)*, 11.76 (s, 0.3H)*, 11.46 (s, 1H), 8.05 (s, 1H), 7.86 (s, 0.3H)*, 7.72 (s, 1H), 7.53–7.36 (m, 7H), 7.22 (s, 0.3H)*, 6.83 (s, 1H), 6.72 (s, 0.3H)*, 6.63 (s, 1H), 6.27 (s, 0.3H)*, 4.25 (q, J = 7.1 Hz, 2H), 1.29 (t, J = 7.1 Hz, 3H); ^{13}C NMR (100 MHz $(CD_3)_2SO$) δ 160.49, 158.43, 139.85, 134.79, 133.47, 132.87, 130.06, 129.19, 128.98, 128.35, 127.35, 126.98, 124.76, 122.35, 117.90, 116.71, 114.98, 113.40, 110.31, 60.39, 14.83; ν_{max}/cm^{-1} 3252, 1683, 2852, 1642, 1544, 1228; HRMS (ESI) m/z [M + H]$^+$ calcd for $C_{23}H_{20}O_3N_4{}^{79}Br$ 479.0713; found 479.0714.

* Rotamer.

^{1}H NMR (600 MHz $(CD_3)_2SO$, 90 °C) δ 11.84 (s, 2H), 11.08 (s, 1H), 8.03 (s, 1H), 7.69 (d, J = 1.9 Hz, 1H), 7.53–7.50 (m, 3H), 7.6 (t, J = 7.6 Hz, 2H), 7.40 (dd, J = 8.7, 1.9 Hz, 1H), 7.35 (t, J = 6.8 Hz, 1H), 6.81 (d, J = 3.9 Hz, 1H), 6.54 (s, 1H), 4.29 (q, J = 7.1 Hz, 2H), 1.32 (t, J = 7.1 Hz, 3H).

4.1.16. Ethyl (*E*)-5-((2-(5-bromo-3-phenyl-1*H*-indole-2-carbonyl)hydrazono)methyl)-1*H*-pyrrole-3-carboxylate (3j). Yellow solid (0.084 g, 0.18 mmol, 69%); mp 230 °C decomposed; ^{1}H NMR (600 MHz $(CD_3)_2SO$) δ 12.11 (s, 2H), 11.27 (s, 1H), 7.89 (s, 1H), 7.68 (s, 1H), 7.47–7.30 (m, 8H), 6.76 (s, 1H), 4.13 (q, J = 7.1 Hz, 2H), 1.20 (t, J = 7.1 Hz, 3H); ^{13}C NMR (100 MHz $(CD_3)_2SO$) δ 163.55, 157.96, 139.68, 134.36, 133.05, 129.57, 128.96, 128.62, 128.26, 127.89, 127.28, 126.92, 126.51, 121.92, 117.16, 116.54, 114.54, 113.60, 112.99, 59.29, 14.40; ν_{max}/cm^{-1} 3320, 2976, 1686, 1538, 1210; HRMS (ESI) m/z [M + H]$^+$ calcd for $C_{23}H_{20}O_3N_4{}^{79}Br$ 479.0713; found 479.0711.

4.1.17. (*E*)-5-((2-(5-Bromo-3-phenyl-1*H*-indole-2-carbonyl) hydrazono)methyl)-1*H*-pyrrole-2-carboxylic acid (3l). Yellow solid (0.068 g, 0.15 mmol, 60%); mp 227 °C decomposed; ^{1}H NMR (400 MHz $(CD_3)_2SO$) δ 12.15 (s, 1H), 12.05 (s, 1H), 11.35 (s, 1H), 7.93 (s, 1H), 7.62 (s, 1H), 7.43–7.26 (m, 8H), 6.69 (s, 1H), 6.53 (s, 1H); ^{13}C NMR (100 MHz $(CD_3)_2SO$) δ 161.55, 158.08, 139.56, 134.39, 133.06, 131.95, 129.67, 128.76, 128.62, 127.98, 126.98, 126.60, 125.42, 121.96, 117.52, 116.09, 114.60, 113.02, 110.06; ν_{max}/cm^{-1} 3312, 3151, 1692, 1637, 1491, 1209; HRMS (ESI) m/z [M + H]$^+$ calcd for $C_{21}H_{16}O_3N_4{}^{79}Br$ 451.0400; found 451.0400.

4.1.18. (*E*)-5-((2-(5-Bromo-3-phenyl-1*H*-indole-2-carbonyl) hydrazono)methyl)-1*H*-pyrrole-3-carboxylic acid (3m). Yellow solid (0.062 g, 0.14 mmol, 58%); mp 260 °C decomposed; ^{1}H NMR (600 MHz $(CD_3)_2SO$) δ 12.14 (s, 1H), 12.05 (s, 1H), 11.93 (s, 1H), 11.26 (s, 1H), 7.91 (s, 1H), 7.70 (s, 1H), 7.49–7.32 (m, 8H), 6.75 (s, 1H); ^{13}C NMR (100 MHz $(CD_3)_2SO$) δ 165.04, 157.89, 139.84, 134.33, 133.04, 129.54, 129.02, 128.59, 128.02, 127.87, 127.23, 126.89, 126.46, 121.89, 117.41, 117.07, 114.51, 113.96, 112.96; ν_{max}/cm^{-1} 3217, 1670, 1636, 1549, 1200; HRMS (ESI) m/z [M + H]$^+$ calcd for $C_{21}H_{16}O_3N_4{}^{79}Br$ 451.0400; found 451.0395.

© 2025 The Author(s). Published by the Royal Society of Chemistry

Open Access Article. Published on 27 June 2025. Downloaded on 12/13/2025 6:15:48 PM. This article is licensed under a Creative Commons Attribution 3.0 Unported Licence.

4.1.19. (*E*)-5-Bromo-*N*′-((5-(morpholine-4-carbonyl)-1*H*-pyrrol-2-yl)methylene)-3-phenyl-1*H*-indole-2-carbohydrazide (3n). Yellow solid (0.11 g, 0.21 mmol, 81%); mp 178–180 °C; ^{1}H NMR (600 MHz $(CD_3)_2SO$) δ 12.10 (s, 1H), 11.92 (s, 1H), 11.31 (s, 1H), 7.98 (s, 1H), 7.68 (s, 1H), 7.48–7.32 (m, 7H), 6.55 (s, 1H), 6.52 (s, 1H), 3.62 (s, 4H), 3.58 (t, J = 4.2 Hz, 4H); ^{13}C NMR (100 MHz $(CD_3)_2SO$) δ 161.05, 157.90, 139.71, 134.33, 133.06, 129.77, 129.63, 128.88, 128.58, 127.93, 126.99, 126.91, 126.50, 121.91, 117.30, 114.53, 113.35, 112.96, 109.87, 66.22; ν_{max}/cm^{-1} 3213, 3054, 2856, 1613, 1489, 1233; HRMS (ESI) m/z $[M + H]^+$ calcd for $C_{25}H_{23}O_3N_5{}^{79}Br$ 520.0979; found 520.0981.

4.1.20. (*E*)-5-Bromo-*N*′-((5-nitro-1*H*-pyrrol-2-yl)methylene)-3-phenyl-1*H*-indole-2-carbohydrazide (3p). Yellow solid (0.092 g, 0.20 mmol, 74%); mp 140 °C decomposed; ^{1}H NMR (600 MHz $(CD_3)_2SO$) δ 13.64 (s, 1H), 13.31 (s, 0.4H)*, 12.19 (s, 1H), 11.98 (s, 0.4H)*, 11.72 (s, 1H), 8.05 (s, 1H), 7.74 (s, 1H), 7.50–7.37 (m, 7H), 7.20 (s, 1H), 7.08 (s, 0.4H)*, 6.74 (s, 1H), 6.29 (s, 0.4H)*; ^{13}C NMR (150 MHz $(CD_3)_2SO$) δ 158.17, 138.41, 137.96, 134.43, 133.36, 132.90, 129.66, 128.55, 128.37, 127.86, 126.97, 126.74, 122.00, 117.93, 114.59, 113.05, 112.79, 110.30; ν_{max}/cm^{-1} 3307, 1645, 1538, 1277; HRMS (ESI) m/z $[M + H]^+$ calcd for $C_{20}H_{15}O_3N_5{}^{79}Br$ 452.0353; found 452.0352.

* Rotamer.

^{1}H NMR (600 MHz $(CD_3)_2SO$, 90 °C) δ 13.23 (s, 1H), 11.88 (s, 1H), 11.36 (s, 1H), 8.03 (s, 1H), 7.70 (d, J = 1.9 Hz, 1H), 7.52–7.50 (m, 3H), 7.45 (t, J = 7.6 Hz, 2H), 7.40 (dd, J = 8.7, 1.9 Hz, 1H), 7.35 (t, J = 7.4 Hz, 1H), 7.14 (d, J = 4.3 Hz), 6.62 (s, 1H).

4.1.21. (*E*)-5-Bromo-*N*′-((4-nitro-1*H*-pyrrol-2-yl)methylene)-3-phenyl-1*H*-indole-2-carbohydrazide (3q). Yellow solid (0.056 g, 0.12 mmol, 46%); mp 302 °C decomposed; ^{1}H NMR (400 MHz $(CD_3)_2SO$) δ 12.72 (s, 1H), 12.17 (s, 1H), 11.47 (s, 1H), 7.95 (s, 1H), 7.90 (s, 1H), 7.72 (s, 1H), 7.49–7.33 (m, 7H), 7.07 (s, 1H); ^{13}C NMR (100 MHz $(CD_3)_2SO$) δ 158.08, 138.74, 137.00, 134.38, 132.96, 129.53, 128.68, 128.56, 128.05, 127.83, 126.90, 126.56, 123.80, 121.92, 117.40, 114.54, 112.98, 107.54; ν_{max}/cm^{-1} 3312, 3138, 1640, 1559, 1285; HRMS (ESI) m/z $[M + H]^+$ calcd for $C_{20}H_{15}O_3N_5{}^{79}Br$ 452.0353; found 452.0352.

4.1.22. (*E*)-5-Bromo-*N*′-((3,5-dimethyl-4-nitro-1*H*-pyrrol-2-yl)methylene)-3-phenyl-1*H*-indole-2-carbohydrazide (3r). Brown solid (0.096 g, 0.2 mmol, 77%); mp 181 °C decomposed; ^{1}H NMR (600 MHz $(CD_3)_2SO$) δ 12.33 (s, 1H), 12.15 (s, 1H), 11.28 (s, 1H), 8.02 (s, 1H), 7.70 (s, 1H), 7.49–7.30 (m, 7H), 2.51 (s, 3H), 2.23 (s, 3H); ^{13}C NMR (100 MHz $(CD_3)_2SO$) δ 157.81, 137.85, 137.48, 134.39, 133.00, 132.71, 129.55, 128.92, 128.61, 127.85, 126.91, 126.54, 122.00, 121.93, 119.36, 117.20, 114.53, 113.03, 13.73, 10.30; ν_{max}/cm^{-1} 3254, 1620, 1545, 1359; HRMS (ESI) m/z $[M + H]^+$ calcd for $C_{22}H_{19}O_3N_5{}^{79}Br$ 480.0666; found 480.0665.

4.1.23. Ethyl (*E*)-4-((2-(5-bromo-3-phenyl-1*H*-indole-2-carbonyl)hydrazono)methyl)-1*H*-pyrrole-2-carboxylate (3v). White solid (0.07 g, 0.15 mmol, 60%); mp 248–250 °C; ^{1}H NMR (400 MHz $(CD_3)_2SO$) δ 12.18 (s, 1H), 12.07 (s, 1H), 11.07 (s, 1H), 7.92 (s, 1H), 7.67 (s, 1H), 7.48_7.30 (m, 8H), 7.00 (s, 1H), 4.23 (q, J = 7.1 Hz, 2H), 1.26 (t, J = 7.1 Hz, 3H); ^{13}C NMR (100 MHz $(CD_3)_2SO$) δ 160.19, 157.78, 143.19, 134.28, 133.10, 129.60, 129.14, 128.58, 127.97, 126.90, 126.40, 125.86, 123.75, 121.85, 120.51, 116.98, 114.49, 112.92, 112.30, 59.97, 14.33; ν_{max}/cm^{-1} 3268, 3064, 2982, 1690, 1659, 1543, 1237; HRMS (ESI) m/z $[M + H]^+$ calcd for $C_{23}H_{20}O_3N_4{}^{79}Br$ 479.0713; found 479.0715.

4.1.24. (*E*)-4-((2-(5-Bromo-3-phenyl-1*H*-indole-2-carbonyl)hydrazono)methyl)-1*H*-pyrrole-2-carboxylic acid (3w). Pale yellow solid (0.079 g, 0.18 mmol, 69%); mp 277 °C decomposed; ^{1}H NMR (400 MHz $(CD_3)_2SO$) δ 12.03 (s, 1H), 12.00 (s, 1H), 11.00 (s, 1H), 7.88 (s, 1H), 7.63 (s, 1H), 7.44–7.26 (m, 8H), 6.91 (s, 1H); ^{13}C NMR (100 MHz $(CD_3)_2SO$) δ 161.69, 157.79, 143.50, 134.30, 133.13, 129.63, 129.18, 128.62, 128.01, 126.94, 126.43, 125.58, 124.75, 121.88, 120.37, 117.00, 114.52, 112.95, 111.97; ν_{max}/cm^{-1} 3311, 3133, 1697, 1636, 1555, 1240; HRMS (ESI) m/z $[M + H]^+$ calcd for $C_{21}H_{16}O_3N_4{}^{79}Br$ 451.0400; found 451.0397.

4.1.25. (*E*)-5-Bromo-*N*′-((5-(morpholine-4-carbonyl)-1*H*-pyrrol-3-yl)methylene)-3-phenyl-1*H*-indole-2-carbohydrazide (3x). Pale yellow solid (0.107 g, 0.20 mmol, 83%); mp 282–284 °C; ^{1}H NMR (600 MHz $(CD_3)_2SO$) δ 12.07 (s, 1H), 11.80 (s, 1H), 11.02 (s, 1H), 7.91 (s, 1H), 7.67 (s, 1H), 7.47–7.26 (m, 8H), 6.73 (s, 1H), 3.66 (s, 4H), 3.59 (t, J = 4.8 Hz, 4H); ^{13}C NMR (100 MHz $(CD_3)_2SO$) δ 160.96, 157.69, 143.68, 134.28, 133.11, 129.58, 129.23, 128.59, 127.95, 126.89, 126.37, 125.80, 124.23, 121.84, 119.59, 116.86, 114.49, 112.92, 108.76, 66.23; ν_{max}/cm^{-1} 3238, 2853, 1631, 1596, 1556, 1252; HRMS (ESI) m/z $[M + H]^+$ calcd for $C_{25}H_{23}O_3N_5{}^{79}Br$ 520.0979; found 520.0980.

4.2. NCI60 screening

The synthesized compounds were evaluated their anticancer properties by submitted to National Cancer Institute 60 human tumour cell lines (NCI60) screening program in the USA.

4.2.1. One-dose screen. The one-dose experimental protocol followed the method described in this literature.[28] First, all compounds were tested at a single concentration (10 μM) across the entire NCI60 panel. The results of this assay indicate the growth relative to no-drug control and the number of cells at time zero. This method allows for the detection of growth inhibition (values between 0 to 100) and lethality (value below 0).

4.2.2. Five-dose screen. The five-dose experimental protocol followed the method described in this literature.[28] Compounds that displayed significant results in the single-dose screen were selected for further experiment across the 60 cell panel at five concentration levels (10 nM, 100 nM, 1 μM, 10 μM and 100 μM). Briefly, the cancer screening panels were cultured in RPMI 1640 medium supplemented with 5% fetal bovine serum and 2 mM L-glutamine. First, cells were plated into 96-well plates at densities in range 5000 to 40 000 cells/well and incubated at 37 °C for 24 hours. After incubation, some plates were treated with trichloroacetic acid (TCA) to determine the time of drug addition (T_z) for each cell line. The plates containing the test compounds at five different concentrations were incubated for 48 hours, fixed, stained with sulforhodamine B (SRB), and incubated at room temperature for 10 minutes. An automate plate was used to measure the absorbance at a wavelength of 515 nm. The percentage of growth inhibition was calculated by use the absorbance from time zero (T_z), control growth (C), and test growth in the presence of drug at the five concentration levels (T_i) using this equation.

Open Access Article. Published on 27 June 2025. Downloaded on 12/13/2025 6:15:48 PM. This article is licensed under a Creative Commons Attribution 3.0 Unported Licence.

$[(T_i - T_z)/(C - T_z)] \times 100$ for concentrations which $T_i \geq T_z$

$[(T_i - T_z)/T_z] \times 100$ for concentration which $T_i < T_z$

The results are reported as Growth Inhibition at 50% (GI_{50}), Total Growth Inhibition (TGI), and Median Lethal Concentration (LC_{50}).

4.3. Tubulin polymerisation assay

The tubulin polymerisation experimental protocol followed the method described in this literature.[28] The experimental was using fluorescence-based assay kit (Cytoskeleton, catalog no. BK011P). In Brief, 5 μL of test compounds was added to a 96-well plate, then mix with 50 μL of a solution containing porcine brain tubulin (2 mg mL^{-1}) in buffer with 20% glycerol and 1 mM GTP. A microplate reader (Varioskan™ LUX multimode microplate reader, Thermo Scientific™) was used to measure fluorescence intensity every 60 seconds for 60 minutes, with excitation at 360 nm and emission at 450 nm, maintained at 37 °C throughout the experiment.

4.4. Cell cycle

A549 human non-small cell lung cancer cell line (ATCC CCL-185) was purchased from American Type Culture Collection (Rockville, MD, USA). Analysis of cell cycle phase distribution was performed as previously described.[40] Briefly, A549 cells in 6-well plate (1×10^5 cells per well) were treated with test compound (or 0.2% DMSO for control). After 24 h treatment, the treated cells were harvested and subjected to cell cycle analysis using Muse Cell Cycle Assay kit (Luminex, Austin, TX, USA) and analyzed with Muse Cell Analyzer™ with (Luminex). The number of cells in each cell cycle phase was expressed as percentage of total cells.

4.5. Aromatase inhibition assay

Aromatase enzyme was purchased from GENTEST, Woburn, MA01801, USA (Supersom human CYP19+oxidoreductase, baculovirus/insect cell-expressed; Product No. 456260). The aromatase inhibitory activity was performed using Human CYP19 enzymes and DBF as a fluorometric substrate as described by Stresser, *et al.*[41] with minor modifications. The mixture, containing 100 μL of cofactor/serial dilution buffer was pre-incubated in 37 °C for 10 min. The reaction was initiated by addition of 100 μL of enzyme/substrate and 10 μL of test compounds (in 10% DMSO) or 10% DMSO as solvent control or 5 μM letrozole (6.3 nM final concentration) as positive control. After incubation at 37 °C for 30 min, the reaction was stopped by addition of 50 μL of 2.2 M NaOH. Fluorescence signal was monitored using an excitation wavelength of 490 nm and emission wavelength of 530 nm. The test compounds showing inhibition >50% were expressed as the half-maximal inhibitory concentration (IC_{50}).

4.6. Cytotoxicity assay

T47D (ATCC HTB-133) was purchased from Biomedia (Thailand) Co., LTD. L929 (ATCC CCL-1) was received as a gift from Prof. Tanapat Palaga, Department of Microbiology, Faculty of Science, Chulalongkorn University, Bangkok, Thailand. The cells were cultured in Dulbecco's Modified Eagle's Medium (DMEM; Gibco) supplemented with 10% fetal bovine serum (FBS; HyClone), 100 U mL^{-1} penicillin and 100 μg mL^{-1} streptomycin (Gibco) at 37 °C with 5% CO_2.

The antiproliferative activity was determined by MTT assay. Briefly, the cells were plated into a 96-well microplate at the density of 10 000 cells per well. The cells were allowed to grow overnight before treated with the solutions of compounds in culture medium at the designated concentrations for 48 hours. The medium was then replaced with MTT solution (0.5 mg mL^{-1} MTT in culture medium) and incubated for 3 hours. A 100 μL of DMSO was used to dissolve the produced formazan. Absorbance at 570 nm was then measured using a microplate reader (Varioskan™ LUX multimode microplate reader, Thermo Scientific™). Percent viability was calculated relative to the vehicle control (DMSO).

4.7. Molecular docking calculations

The ligands were constructed using Chem3D Pro 12.0 and energy minimized using the MM2 (ref. 42) force field. The tubulin structure was downloaded from the Protein Data Bank (PDB):[43] tubulin (PDB ID: 4O2B, resolution 2.3 Å),[44] as aromatase (PDB ID: 3S7S, resolution 3.2 Å).[45] The protein structure were prepared for the docking simulations, *i.e.*, co-crystallised colchicine and spectator ligands were removed. The centre of the colchicine binding pocket of tubulin, and aromatase binding site were defined at coordinates ($x = 13.222, y = 8.371, z = -23.331$) and ($x = 85.219$, $y = 49.732$, $z = 42.202$), respectively, with 10 Å radius. The docking runs were set at fifty docking runs per ligand with default search efficiency (100%) to permit thorough searches for the best bioactive conformations. Basic amino acids including lysine and arginine were defined as protonated, whilst acidic amino acids including aspartic and glutamic acids were deprotonated. The GoldScore (GS) scoring function was implemented to calculate the binding score and predict the binding modes, which was included in the GOLD version 2023.2.0 software suite.[46] Discovery Studio 4.5 visualizer was used as a visualizer to examine and analyse the predicted binding modes and intermolecular interactions.

4.8. Calculations of physicochemical properties

The Dragon 7.0 software package was automated to calculate the molecular descriptors of the derivatives: MWs, number of HAs and HDs, number of RBs, PSA and *M*logP. The ADMETlab 3.0 web server was automated to predict for the toxicities of the compounds.

Data availability

The data supporting this article have been included as part of the ESI.†

© 2025 The Author(s). Published by the Royal Society of Chemistry

Open Access Article. Published on 27 June 2025. Downloaded on 12/13/2025 6:15:48 PM. This article is licensed under a Creative Commons Attribution 3.0 Unported Licence.

Author contributions

Rungroj Saruengkhanphasit: conceptualization, project administration, methodology, data curation, writing – original draft, writing – review & editing, funding acquisition. Jaruwan Chatwichien: methodology. Lukana Ngiwsara: methodology. Kriengsak Lirdprapamongkol: methodology, writing – review & editing, funding acquisition. Worawat Niwetmarin: methodology, writing – review & editing. Chatchakorn Eurtivong: conceptualization, methodology, writing – review & editing. Prasat Kittakoop: conceptualization, data curation, supervision, writing – review & editing. Jisnuson Svasti: data curation, writing – review & editing. Somsak Ruchirawat: data curation, writing – review & editing.

Conflicts of interest

The authors declare no competing financial interest.

Acknowledgements

This work (Grant No. RGNS 65-207) was supported by Office of the Permanent Secretary, Ministry of Higher Education, Science, Research and Innovation (OPS MHESI), Thailand Science Research and Innovation (TSRI) and Chulabhorn Graduate Institute. Additional supports in part were from the Center of Excellence on Environmental Health and Toxicology (EHT), OPS, Ministry of Higher Education, Science, Research and Innovation; and Thailand Science Research and Innovation (TSRI), Chulabhorn Research Institute (Grant No. 49890/4759797 and 49893/4759807).We thank S. Sitthimonchai from Biological Activity Testing Service, CRI, Thailand, for aromatase assays.

References

1 H. Sung, J. Ferlay, R. L. Siegel, M. Laversanne, I. Soerjomataram, A. Jemal and F. Bray, *Ca-Cancer J. Clin.*, 2021, **71**, 209–249.
2 F. Bray, M. Laversanne, H. Sung, J. Ferlay, R. L. Siegel, I. Soerjomataram and A. Jemal, *Ca-Cancer J. Clin.*, 2024, **74**, 229–263.
3 R. W. Brueggemeier, J. C. Hackett and E. S. Diaz-Cruz, *Endocr. Rev.*, 2005, **26**, 331–345.
4 T. Reinert, B. D. Paula, M. N. Shafaee, P. H. Souza, M. J. Ellis and J. Bines, *Chin. J. Clin. Oncol.*, 2018, **7**, 25.
5 E. Amir, B. Seruga, S. Niraula, L. Carlsson and A. Ocaña, *J. Natl. Cancer Inst.*, 2011, **103**, 1299–1309.
6 A. S. Coates, A. Keshaviah, B. Thürlimann, H. Mouridsen, L. Mauriac, J. F. Forbes, R. Paridaens, M. Castiglione-Gertsch, R. D. Gelber, M. Colleoni, I. Láng, L. D. Mastro, I. Smith, J. Chirgwin, J.-M. Nogaret, T. Pienkowski, A. Wardley, E. H. Jakobsen, K. N. Price and A. Goldhirsch, *J. Clin. Oncol.*, 2007, **25**, 486–492.
7 P. E. Lønning and H. P. Eikesdal, *Endocr.-Relat. Cancer*, 2013, **20**, R183–R201.
8 A. F. Sobral, C. Amaral, G. Correia-da-Silva and N. Teixeira, *J. Steroid Biochem. Mol. Biol.*, 2016, **163**, 1–11.
9 M. A. Jordan and L. Wilson, *Nat. Rev. Cancer*, 2004, **4**, 253–265.
10 T. Fojo and M. Menefee, *Ann. Oncol.*, 2007, **18**, v3–v8.
11 N. Watanabe, Y. Ootawa, K. Kodama, A. Kaide, N. Ootsuka and J. Matsuoka, *Breast Cancer*, 2010, **17**, 247–253.
12 P. A. Young, D. C. Márquez-Garbán, Z. S. Noor, N. Moatamed, D. Elashoff, T. Grogan, T. Romero, H. Sasano, R. Saito, R. Rausch, N. Hamilton, S. M. Dubinett, E. B. Garon and R. J. Pietras, *JTO Clin. Res. Rep.*, 2021, **2**, 100150.
13 M. M. Shaaban, M. Teleb, H. M. Ragab, M. Singh, B. H. Elwakil, L. A. Heikal, D. Sriram and M. A. Mahran, *Bioorg. Chem.*, 2024, **145**, 107179.
14 A. B. Velappan, D. Kesamsetty, D. Datta, R. Ma, N. Hari, S. G. Franzblau and J. Debnath, *Eur. J. Med. Chem.*, 2020, **208**, 112835.
15 J. He and K. Y. Tam, *Drug Discovery Today*, 2024, **29**, 103914.
16 J. P. S. Ferreira, H. M. T. Albuquerque, S. M. Cardoso, A. M. S. Silva and V. L. M. Silva, *Eur. J. Med. Chem.*, 2021, **221**, 113492.
17 N. S. Tibon, C. H. Ng and S. L. Cheong, *Eur. J. Med. Chem.*, 2020, **188**, 111983.
18 T. Liang, L. Cen, J. Wang, M. Cheng, W. Guo, W. Wang, C. Yu, H. Zhang, Y. Wang, Z. Hao, J. Jin, Y. Wu, T. Jiang, Q. Zhu and Y. Xu, *Bioorg. Med. Chem.*, 2023, **96**, 117354.
19 J. Zhang, X. Liu, N. Sa, J.-H. Zhang, Y.-S. Cai, K.-M. Wang, W. Xu, C.-S. Jiang and K.-K. Zhu, *Eur. J. Med. Chem.*, 2024, **269**, 116341.
20 D. Yevale, N. Teraiya, T. Lalwani, M. Dalasaniya, K. Kapadiya, R. K. Ameta, C. B. Sangani and Y.-T. Duan, *Bioorg. Chem.*, 2024, **147**, 107323.
21 S. Kurup, D. Gesinski, K. Assaad and A. Reynolds, *Bioorg. Med. Chem. Lett.*, 2024, **100**, 129612.
22 A. A. Mohamed, S. S. A. El-Hddad, A. K. B. Aljohani, F. Khedr, O. M. Alatawi, D. E. Keshek, S. Ahmed, M. Alsulaimany, S. A. Almadani, K. El-Adl and N. S. Hanafy, *Bioorg. Chem.*, 2024, **143**, 107062.
23 M. K. Verma, C. Samant, R. Kale, S. Patra, N. Mahajan, M. K. Gholve, A. Marisetti, B. Sunkara, A. Naik, M. Shingare, M. Reddy, A. M. Bokare, A. Akarte, S. Koul, P. B. Nigade, V. B. Patil, D. Modi, P. Ahirrao, S. Pawar, S. Kuldharan, L. Dinchhana, M. Mehta, J. Gundu, N. Jana, P. Vidhate, S. C. Mahangare, M. R. Shukla, R. N. Goel, M. Bhonde, R. K. Kamboj and V. P. Palle, *Biochem. Biophys. Res. Commun.*, 2022, **637**, 267–275.
24 G. Ana, P. M. Kelly, A. M. Malebari, S. Noorani, S. M. Nathwani, B. Twamley, D. Fayne, N. M. O'Boyle, D. M. Zisterer, E. F. Pimentel, D. C. Endringer and M. J. Meegan, *Pharmaceuticals*, 2021, **14**, 169.
25 X. Deng, X. Deng, W. Ning, L. Xin, Q. Li, Z. Hu, B. Xie, K. Liang, C. Min, C. Dong, J. Huang and H.-B. Zhou, *J. Med. Chem.*, 2023, **66**, 11094–11117.
26 N. M. O'Boyle, J. K. Pollock, M. Carr, A. J. S. Knox, S. M. Nathwani, S. Wang, L. Caboni, D. M. Zisterer and M. J. Meegan, *J. Med. Chem.*, 2014, **57**, 9370–9382.

© 2025 The Author(s). Published by the Royal Society of Chemistry

Open Access Article. Published on 27 June 2025. Downloaded on 12/13/2025 6:15:48 PM.
This article is licensed under a Creative Commons Attribution 3.0 Unported Licence.

27 R. Saruengkhanphasit, C. Butkinaree, N. Ornnork, K. Lirdprapamongkol, W. Niwetmarin, J. Svasti, S. Ruchirawat and C. Eurtivong, *Bioorg. Chem.*, 2021, **110**, 104795.
28 R. Saruengkhanphasit, L. Ngiwsara, K. Lirdprapamongkol, J. Chatwichien, W. Niwetmarin, C. Eurtivong, P. Kittakoop, J. Svasti and S. Ruchirawat, *RSC Med. Chem.*, 2024, **15**, 2483–2495.
29 H.-Z. Zhang, J. Drewe, B. Tseng, S. Kasibhatla and S. X. Cai, *Bioorg. Med. Chem.*, 2004, **12**, 3649–3655.
30 R. H. Shoemaker, *Nat. Rev. Cancer*, 2006, **6**, 813–823.
31 M. Alvarez, K. Paull, A. Monks, C. Hose, J. S. Lee, J. Weinstein, M. Grever, S. Bates and T. Fojo, *J. Clin. Invest.*, 1995, **95**, 2205–2214.
32 Q. Pan, X. J. Yang, H.-M. Wang, X.-T. Dong, W. Wang, Y. Li and J.-M. Li, *Cell Biochem. Biophys.*, 2012, **62**, 185–191.
33 A. V. Taubenberger, B. Baum and H. K. Matthews, *Front. Cell Dev. Biol.*, 2020, **8**, 687.
34 E. W. Bell and Y. Zhang, *J. Cheminf.*, 2019, **11**, 40.
35 D. Ramírez and J. Caballero, *Molecules*, 2018, **23**, 1038.
36 I. Moriguchi, S. Hirono, Q. Liu, I. Nakagome and Y. Matsushita, *Chem. Pharm. Bull.*, 1992, **40**, 127–130.
37 C. A. Lipinski, F. Lombardo, B. W. Dominy and P. J. Feeney, *Adv. Drug Delivery Rev.*, 2012, **64**, 4–17.
38 D. F. Veber, S. R. Johnson, H.-Y. Cheng, B. R. Smith, K. W. Ward and K. D. Kopple, *J. Med. Chem.*, 2002, **45**, 2615–2623.
39 L. Fu, S. Shi, J. Yi, N. Wang, Y. He, Z. Wu, J. Peng, Y. Deng, W. Wang, C. Wu, A. Lyu, X. Zeng, W. Zhao, T. Hou and D. Cao, *Nucleic Acids Res.*, 2024, **52**, W422–W431.
40 W. Rodphon, P. Laohapaisan, N. Supantanapong, O. Reamtong, L. Ngiwsara, K. Lirdprapamongkol, C. Thongsornkleeb, N. Khunnawutmanothan, J. Tummatorn, J. Svasti and S. Ruchirawat, *ChemMedChem*, 2021, **16**, 3750–3762.
41 D. M. Stresser, S. D. Turner, J. McNamara, P. Stocker, V. P. Miller, C. L. Crespi and C. J. Patten, *Anal. Biochem.*, 2000, **284**, 427–430.
42 N. L. Allinger, *J. Am. Chem. Soc.*, 1977, **99**, 8127–8134.
43 H. M. Berman, J. Westbrook, Z. Feng, G. Gilliland, T. N. Bhat, H. Weissig, I. N. Shindyalov and P. E. Bourne, *Nucleic Acids Res.*, 2000, **28**, 235–242.
44 A. E. Prota, F. Danel, F. Bachmann, K. Bargsten, R. M. Buey, J. Pohlmann, S. Reinelt, H. Lane and M. O. Steinmetz, *J. Mol. Biol.*, 2014, **426**, 1848–1860.
45 D. Ghosh, J. Lo, D. Morton, D. Valette, J. Xi, J. Griswold, S. Hubbell, C. Egbuta, J. Wenhua, J. An and H. M. L. Davies, *J. Med. Chem.*, 2012, **55**, 8464–8476.
46 M. L. Verdonk, J. C. Cole, M. J. Hartshorn, C. W. Murray and R. D. Taylor, *Proteins*, 2003, **52**, 609–623.

© 2025 The Author(s). Published by the Royal Society of Chemistry